5-16-2017

Effects of Temperature and Radiation Dose on Radiation Induced Conductivity

JR Dennison
Utah State Univesity

Recommended Citation

JR Dennison, "Effects of Temperature and Radiation Dose on Radiation Induced Conductivity," Invited Talk, Sandia National Laboratories: Electronic, Optical and Nano Materials Division, Albuquerque, NM May 16, 2017.

Sandia National Laboratories
Albuquerque, NM
May 16, 2017

Effects of Temperature and Radiation Dose on Radiation Induced Conductivity

J.R. Dennison

Materials Physics Group
Physics Department, Utah State University

Rose-Fowler-Vaserberg theory

A Rose by any other name would smell as sweet…

In search of the Holy Grail of the Videcon…

Rose found zero x-ray radiography …

XEROX®

What Is Radiation Induced Conductivity (RIC)?

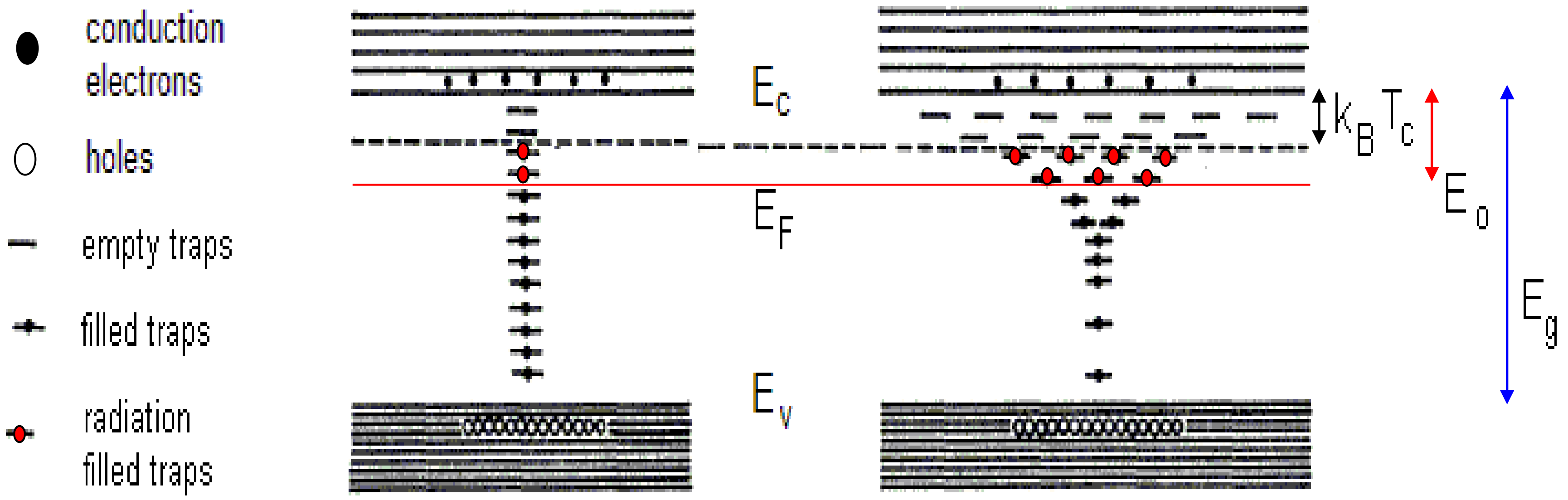

Dose Dependant RIC

$$\sigma_{RIC}(\dot{D}) = k_{RIC} \cdot \dot{D}^{\Delta}$$

Uniform Trap Density

$$\Delta(T) \rightarrow 1$$

$$k(T) \rightarrow k_{RICo}$$

Exponential Trap Density

$$\Delta(T) \rightarrow T_c \big/ T + T_c$$

$$k(T) \rightarrow k_{RIC1}\left[2\left(\frac{m_e k_B T}{2\pi\hbar^2}\right)^{3/2}\left(\frac{m_e^* m_h^*}{m_e\, m_e}\right)^{3/4}\right]^{\frac{T}{T+T_c}}$$

$$\sigma_{RIC}(T,D) = k_{RIC}(T) \cdot D^{\Delta(T)}$$

Radiation Dose Dependence of Conductivity

Radiation-induced conductivity (RIC) is proportional to dosage to the Δ power:

$$\sigma_{RIC}(\dot{D}) = k \cdot \left(\dot{D}\right)^{\Delta}$$

To first order, this does not depend on T or on the incident radiation species, just energy flux.

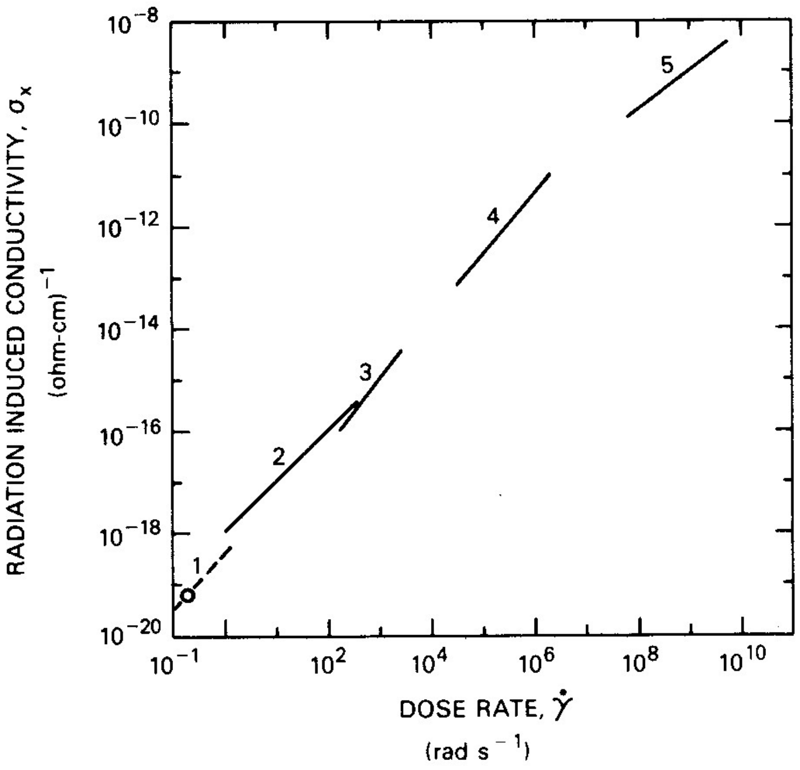

- The RIC versus radiation dose rate for polyethylene terephthalate (Mylar) [Campbell].
- The exponential fit over 10 orders of magnitude for five different studies implies that RIC is largely independent of the beam energy and type of radiation used.
- Only the amount of energy being deposited determines the magnitude of RIC.

Curve Segment	Type of Radiation	Energy	Dose Rate	Mode
1	X-rays	250 keV	0.13 rad/s	steady state
2	X-rays	15 to 30 keV	1 to 400 rad/s	steady state
3	γ-rays	1.17 and 1.33 MeV	200 to 3500 rad/s	steady state
4	pulse reactor neutrons and γ-rays	mixed	6.5×10^4 to 3.8×10^6 R/s	13 ms pulses
5	electrons	30 MeV	5×10^7 to 7×10^9 rad/s	4.5 μs pulses

RIC Dependence on Temperature

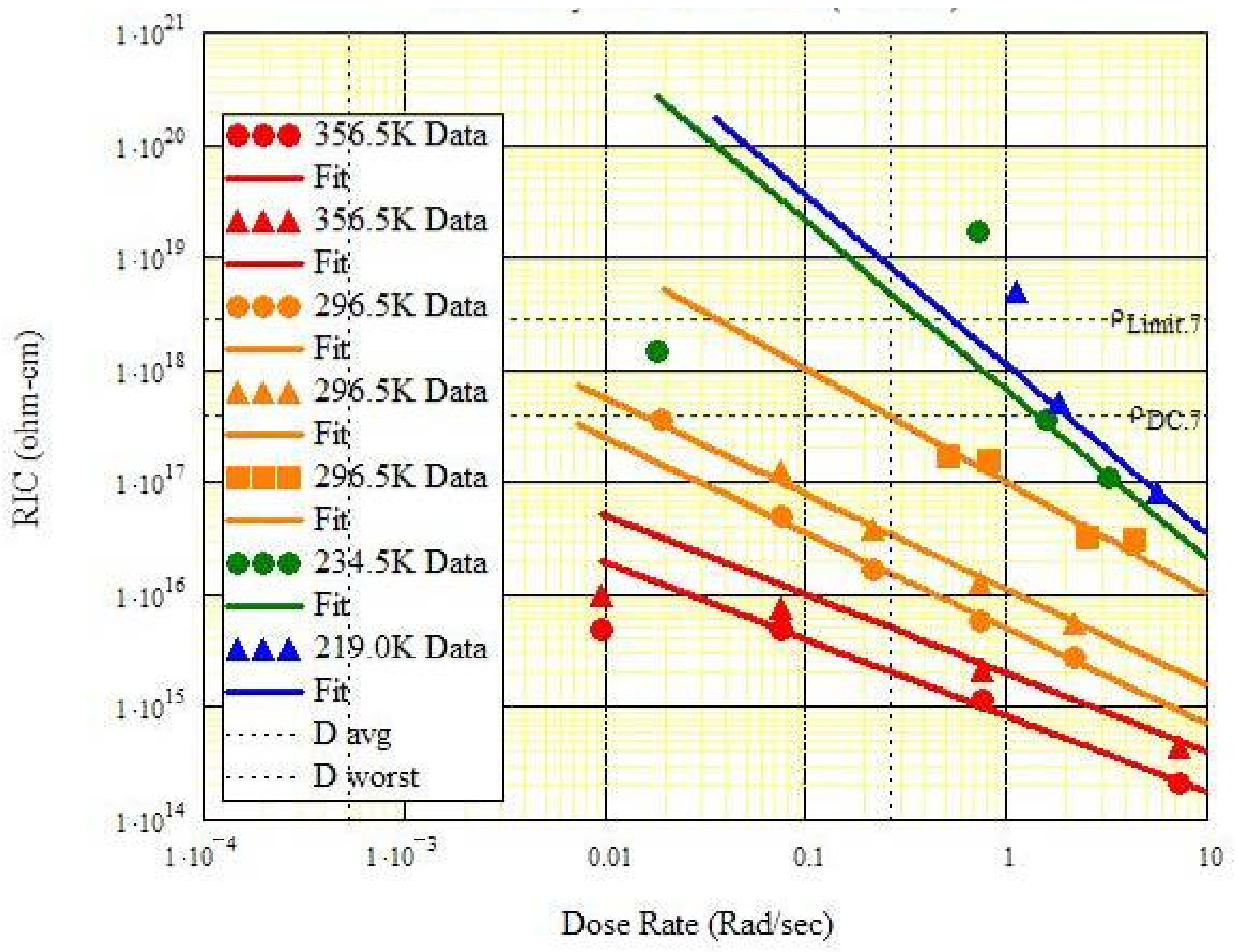

Kapton™ (polyimide)

Family of curves of ρ_{RIC} vs dose rate at various temperatures. Fits are simple power law fits.

$$\sigma_{RIC}(T,D) = k_{RIC}(T)\cdot D^{\Delta(T)}$$

RIC Dependence on Temperature

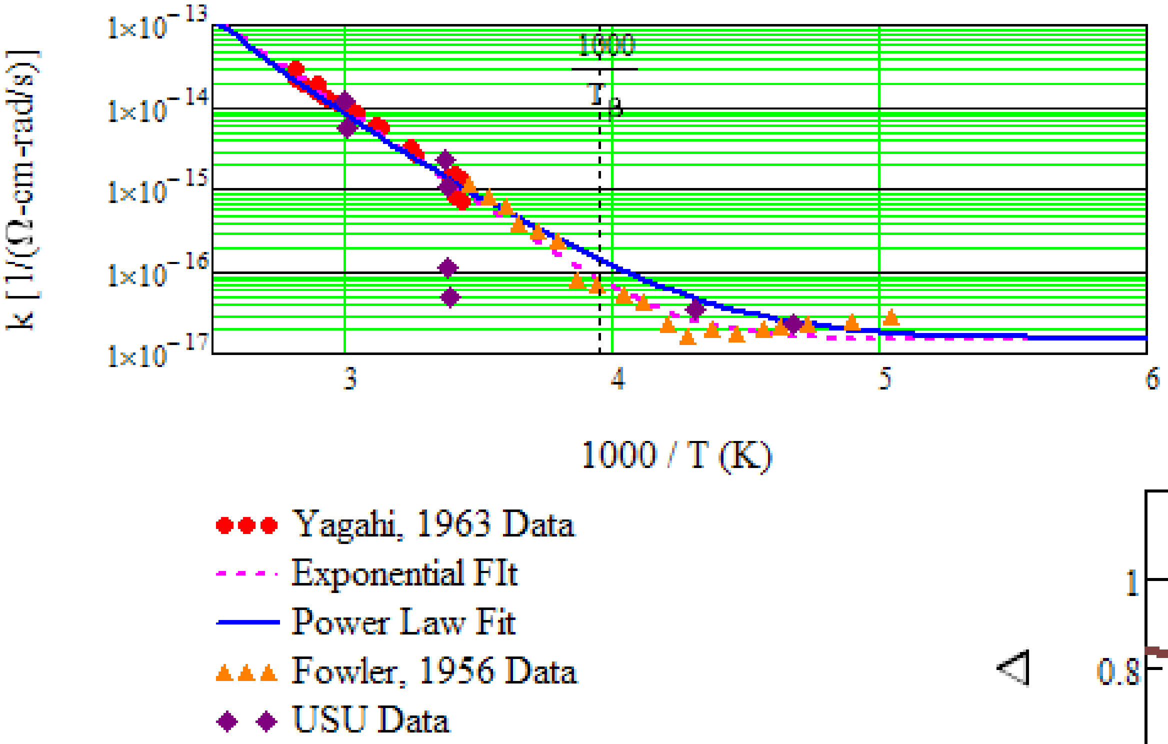

Kapton™ (polyimide)

$$\sigma_{RIC}(T,D) = k_{RIC}(T) \cdot D^{\Delta(T)}$$

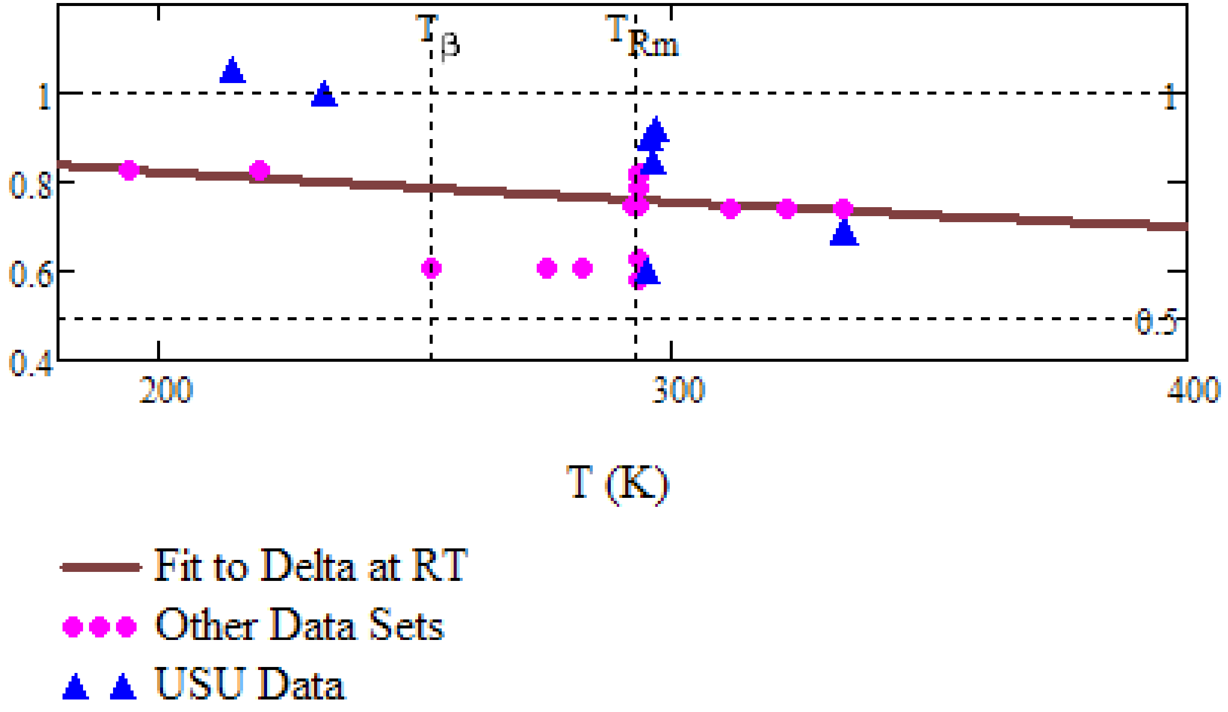

T dependence of RIC coefficients k (Above) and Δ (Right) with $k_o = 1.5 \cdot 10^{-16}$ $(\Omega\text{-cm-Rad/s})^{-1}$, $k_1 = 7.0 \cdot 10^{-29}$ $(\Omega\text{-cm-Rad/s})^{-1}$ and T_c = 230 K.

RIC Is Time Dependant

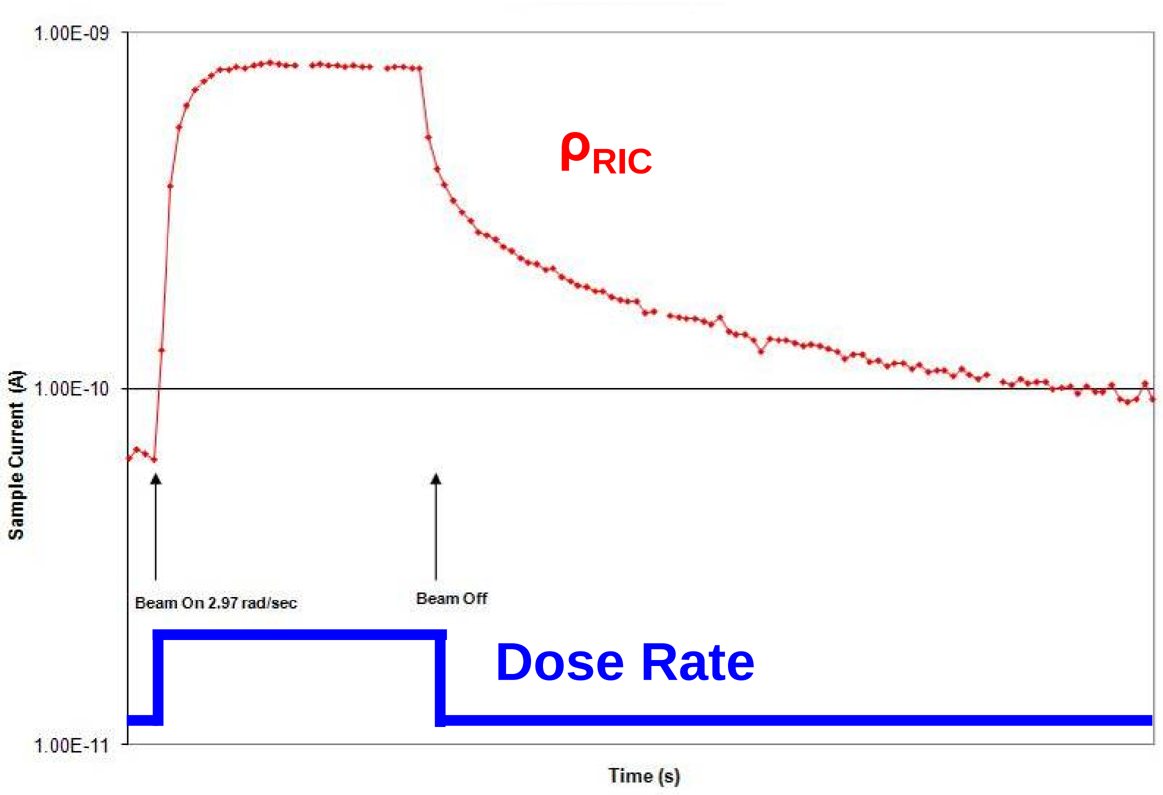

Initial RIC

$$B_{on}(t, \lambda(D,T)) = 1 - e^{-(t - t_{on}) \cdot \lambda(D,T)}$$

Dose Dependent Equilibrium RIC

$$\sigma_{RIC}(T, D) = k_{RIC}(T) \cdot D^{\Delta(T)}$$

Persistent RIC

$$B_{off}(t, T, k(T)) = \frac{1}{1 + k(T) \cdot \frac{t - t_{off}}{T}}$$

Instrumentation

Idaho Accelerator Center RIC Chamber

Radiation Induced Conductivity Measurements

RIC chamber uses a combination of charge injected by a biased surface electrode with simultaneous energy injection by a pulsed penetrating electrons.

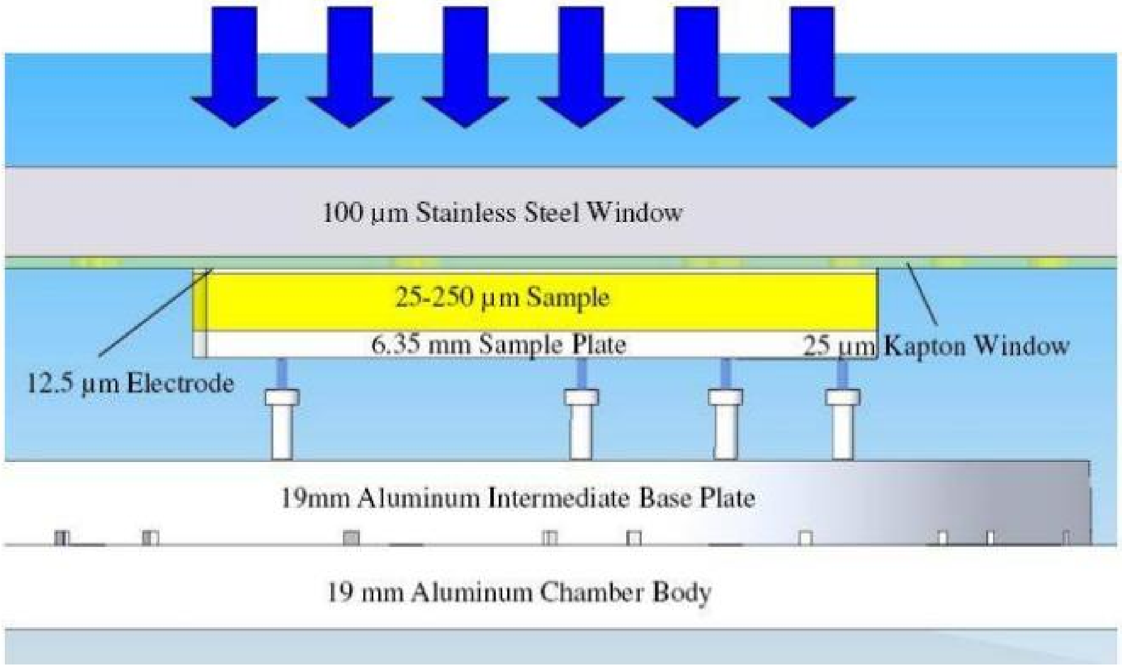

Sample stack cross section

RIC Chamber

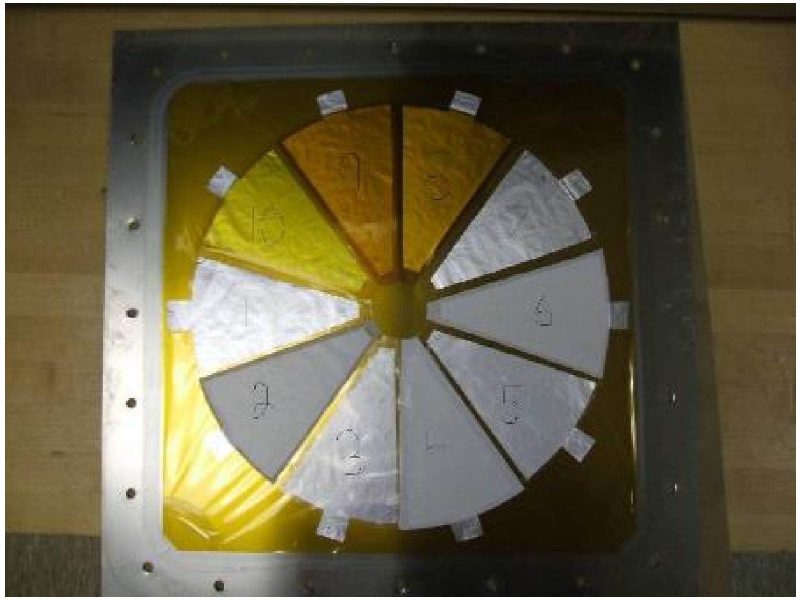

Top view of samples on window

Instrumentation

USU Cryostat RIC Chamber

AFRL RIC Cryostat Chamber

High Energy Electron Gun

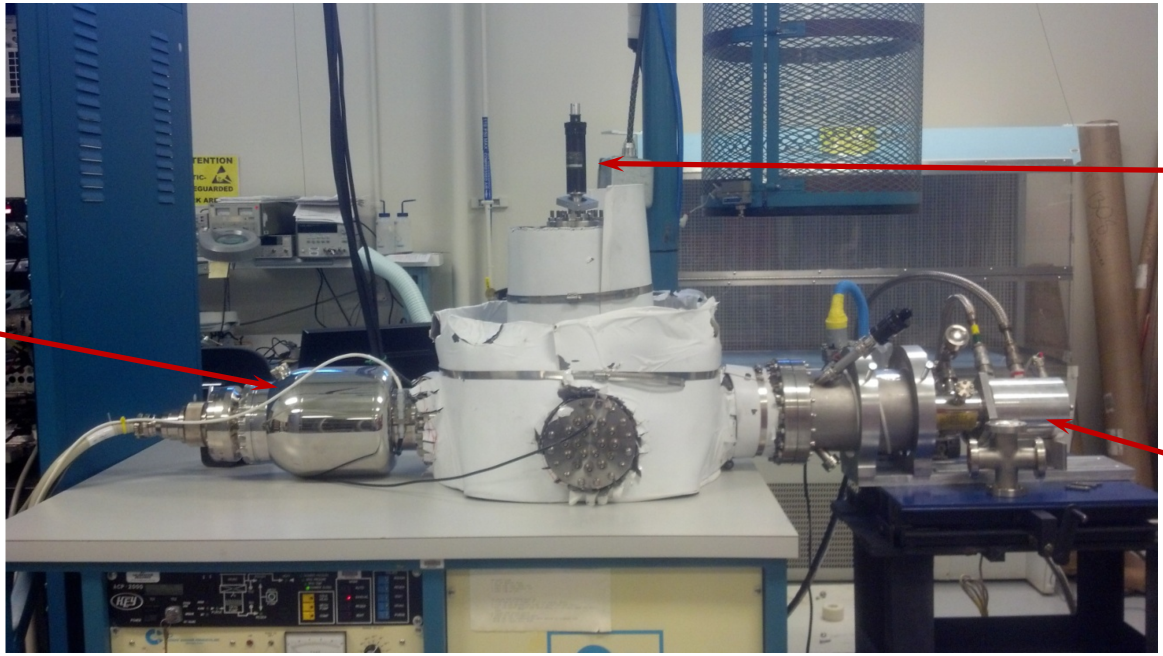

Faraday Cup Z Translation Stage

USU Closed Cycle He Cryostat

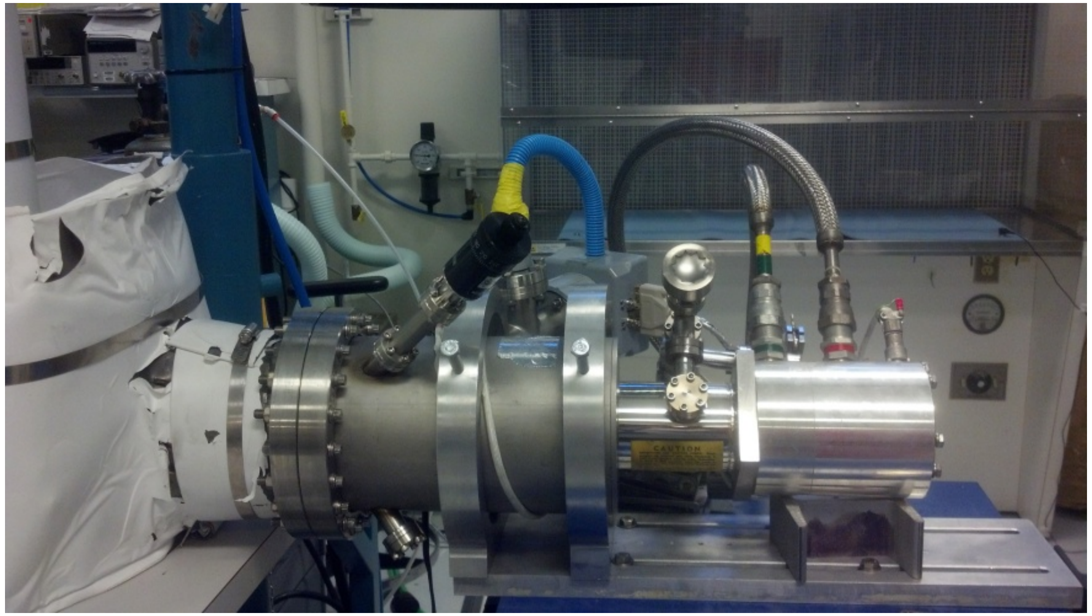

AFRL RIC Cryostat Chamber Cut Away Diagram

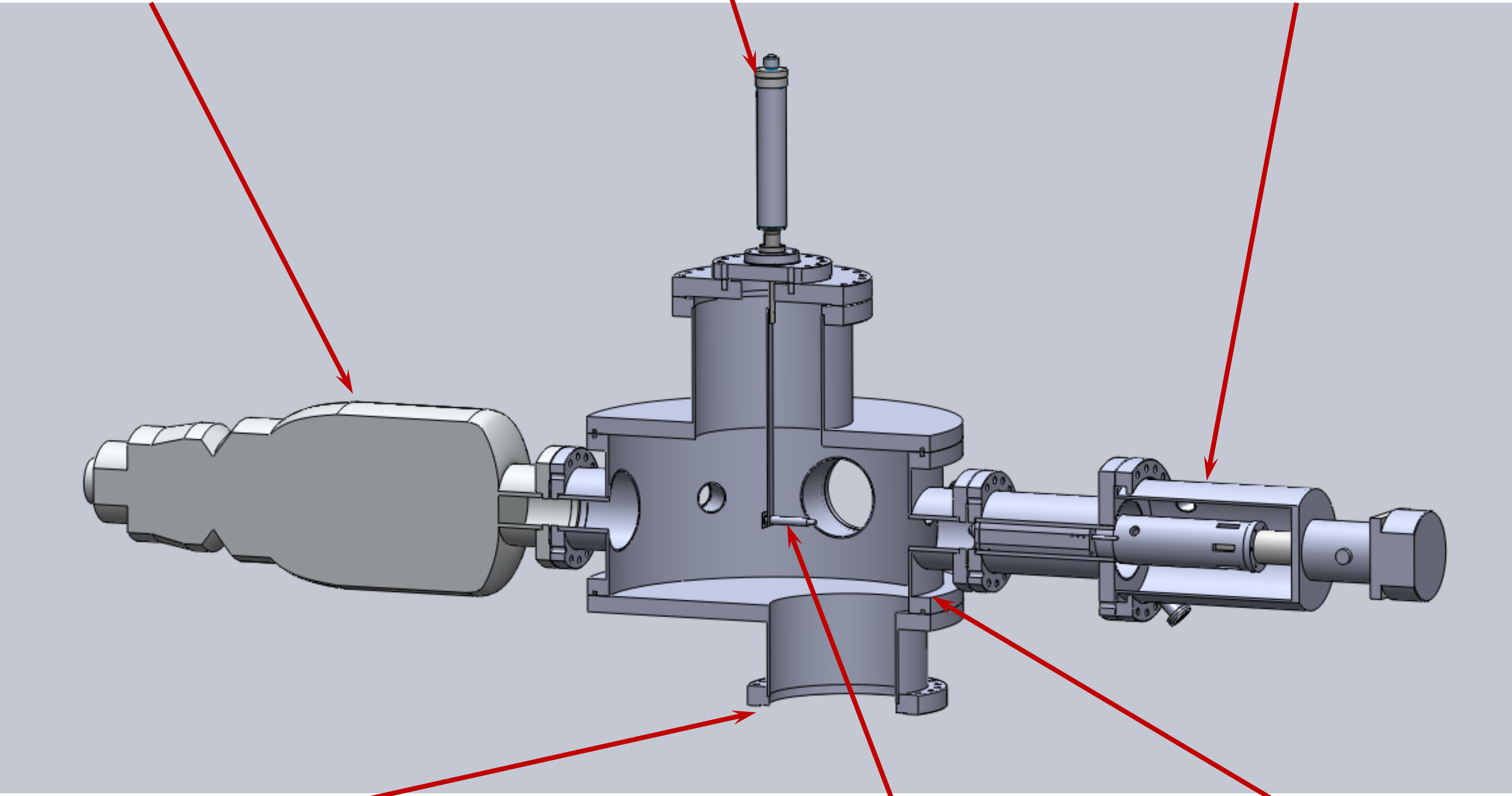

AFRL RIC Closed-Cycle He Refrigerator Sample Stage Design

Cryo Sample Stage Assembly
Cut-Away Views

Expander Module

Cryo shroud

Cryo Shroud Stage (~80 K)

Low T Stage (~30 K)

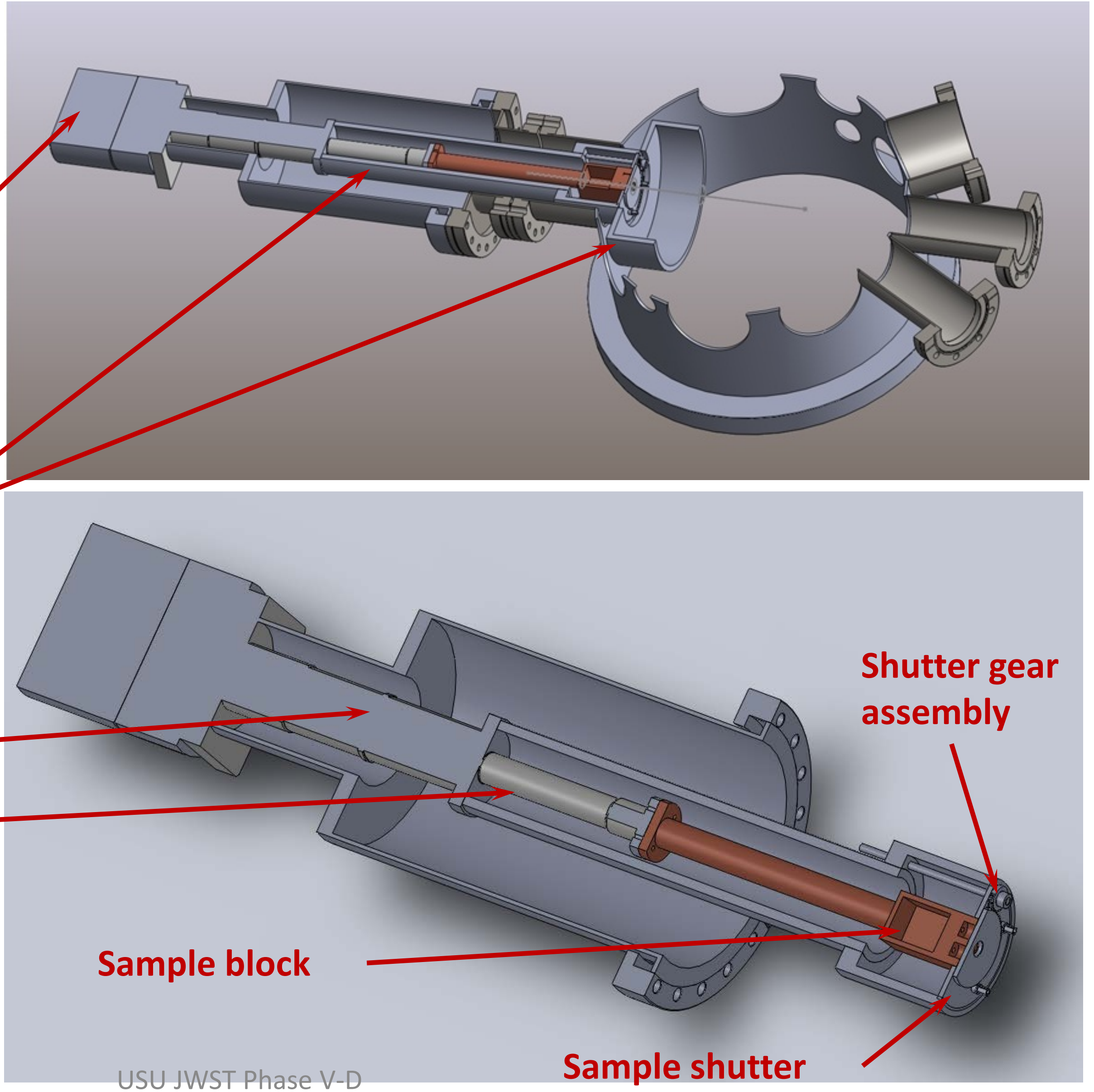

AFRL RIC Closed-Cycle He Refrigerator Sample Stage Design

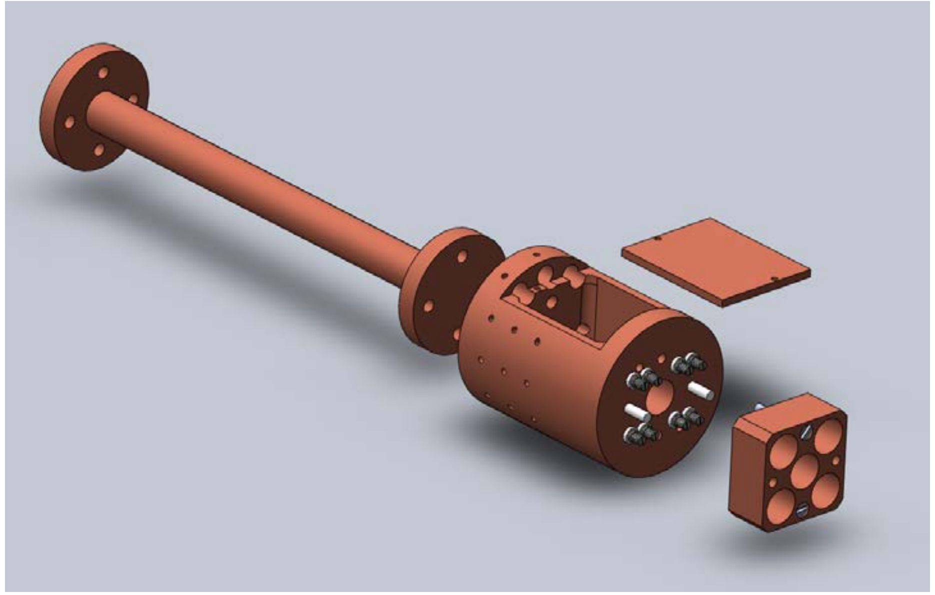

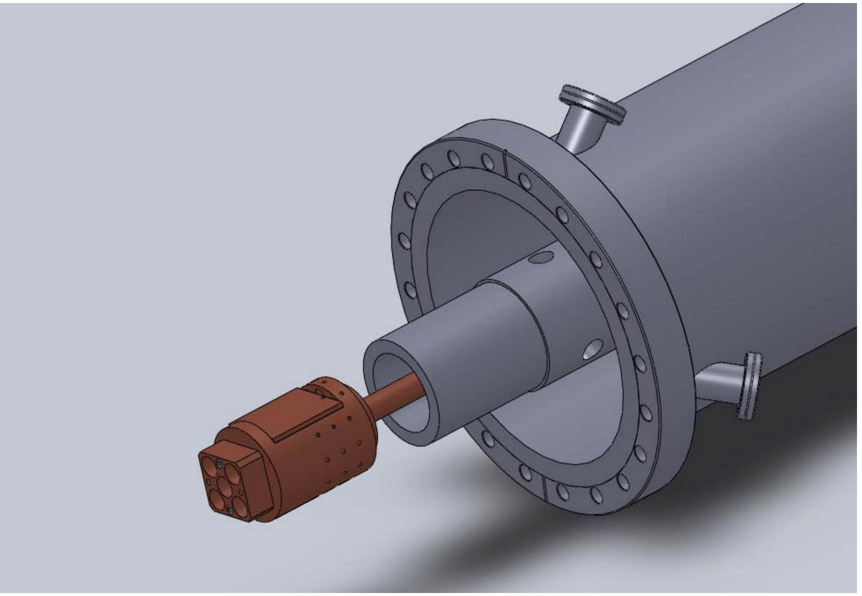

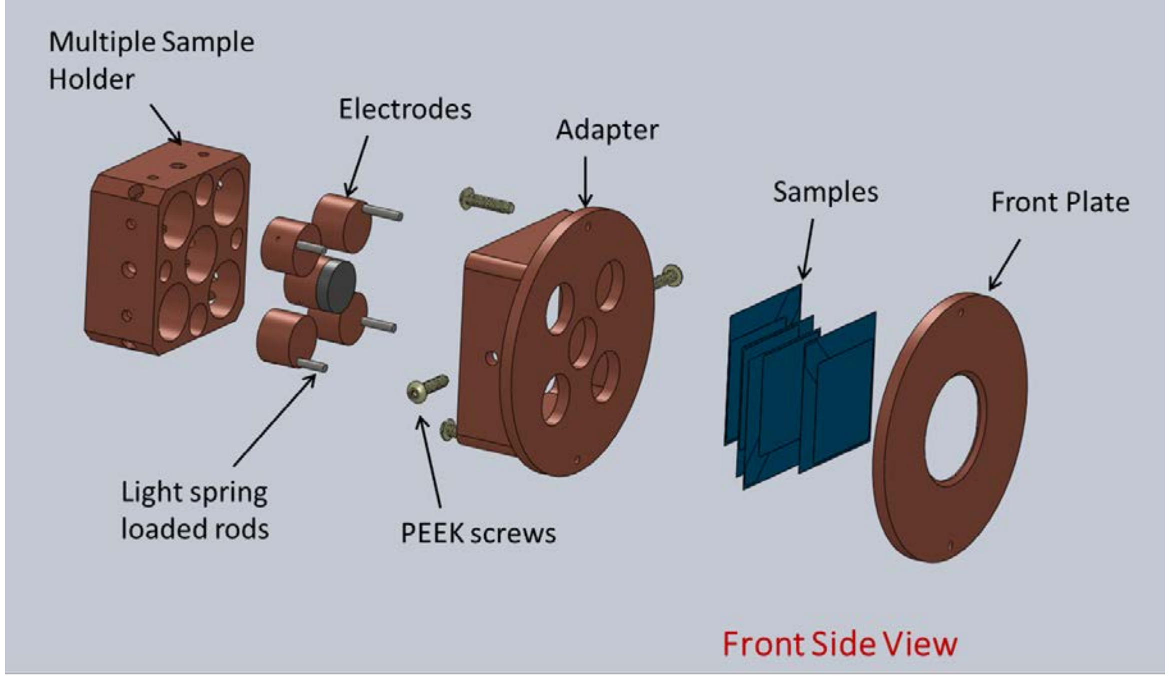

AFRL RIC System Cryostat Block Diagram

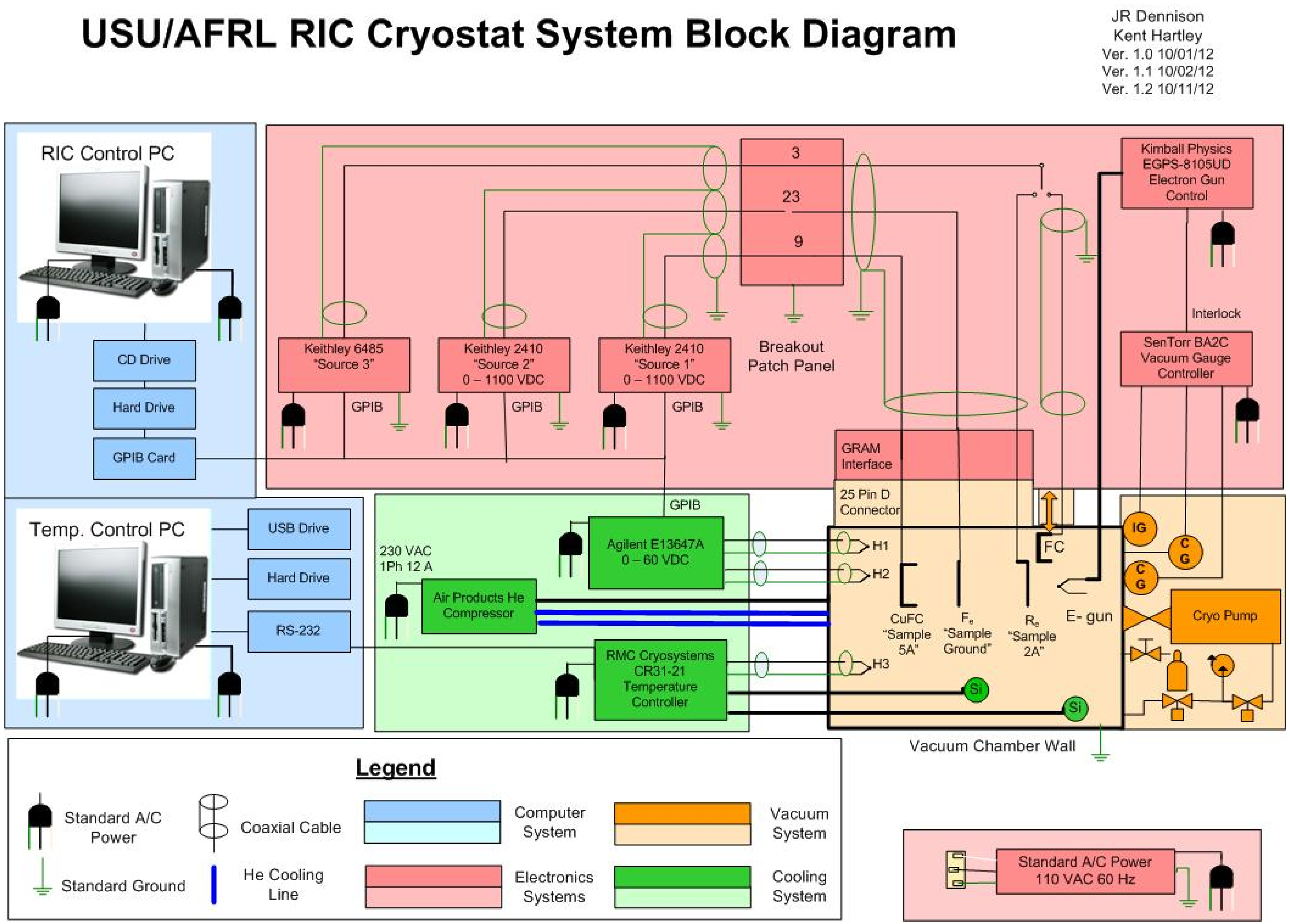

Complementary Responses to Radiation

Modified Joblonski diagram

- VB electrons excited into CB by the high energy incident electron radiation.
- They relax into shallow trap (ST) states, then thermalize into lower available long-lived ST.
- Three paths are possible:

(i) relaxation to deep traps (DT), with concomitant photon emission;
(ii) radiation induced conductivity (RIC), with thermal re-excitation into the CB; or
(iii) non-radiative transitions or e^--h^+ recombination into VB holes.

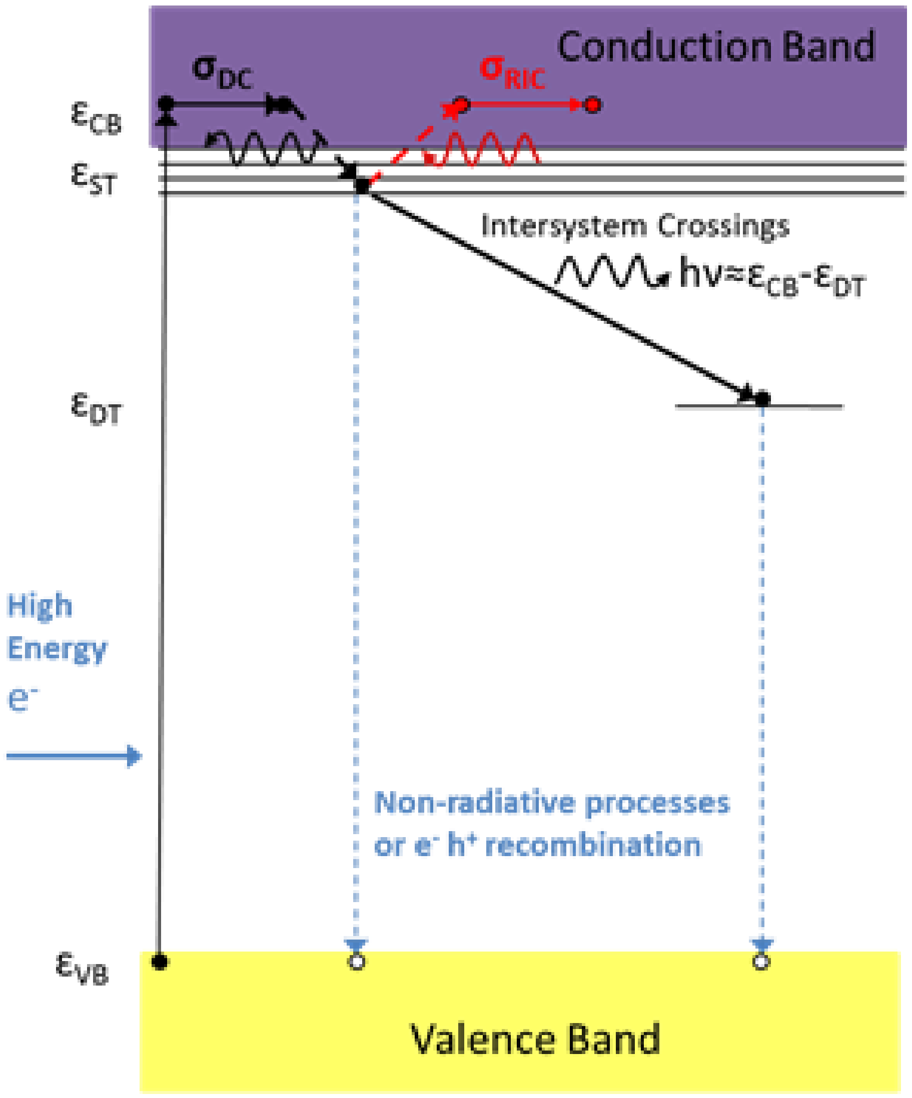

RIC Cryostat Measurements

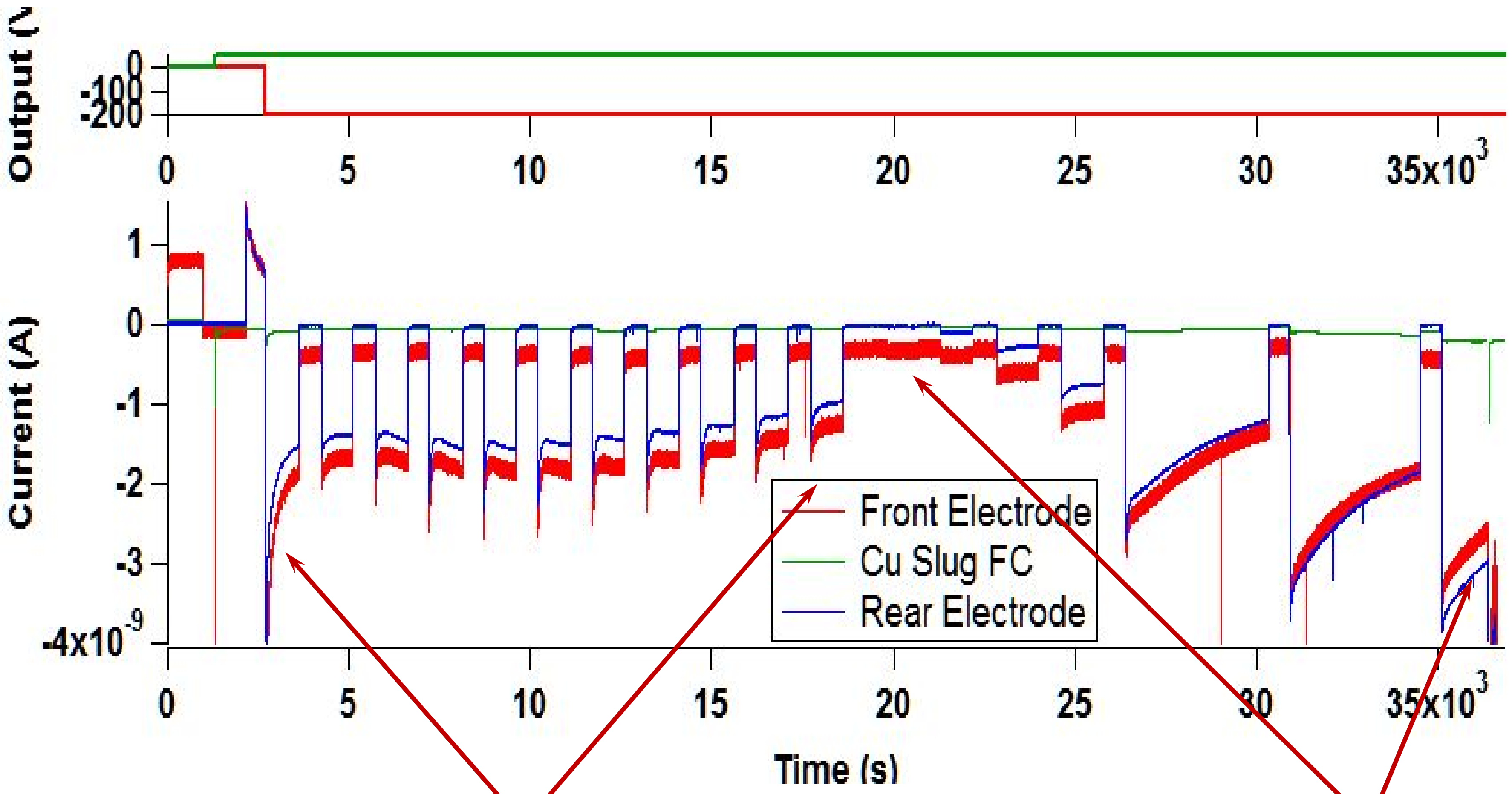

Fused silca

RIC current vs 295 K<T<38 K at constant Dose Rate

RIC curent vs Dose Rate at 40 K

Room T RIC Cryostat System Results

$$k_{plot} := \frac{1}{4.6 \cdot 10^{14} \cdot ohm \cdot cm} = 2.17 \times 10^{-15} \cdot \frac{1}{(ohm \cdot cm)}$$

Fused silca

$$\Delta_{plot} := 1.00 \qquad \rho_{plot}(DR) := \frac{1}{k_{plot}} \cdot \left(\frac{DR}{\frac{RAD}{s}} \right)^{-\Delta_{plot}}$$

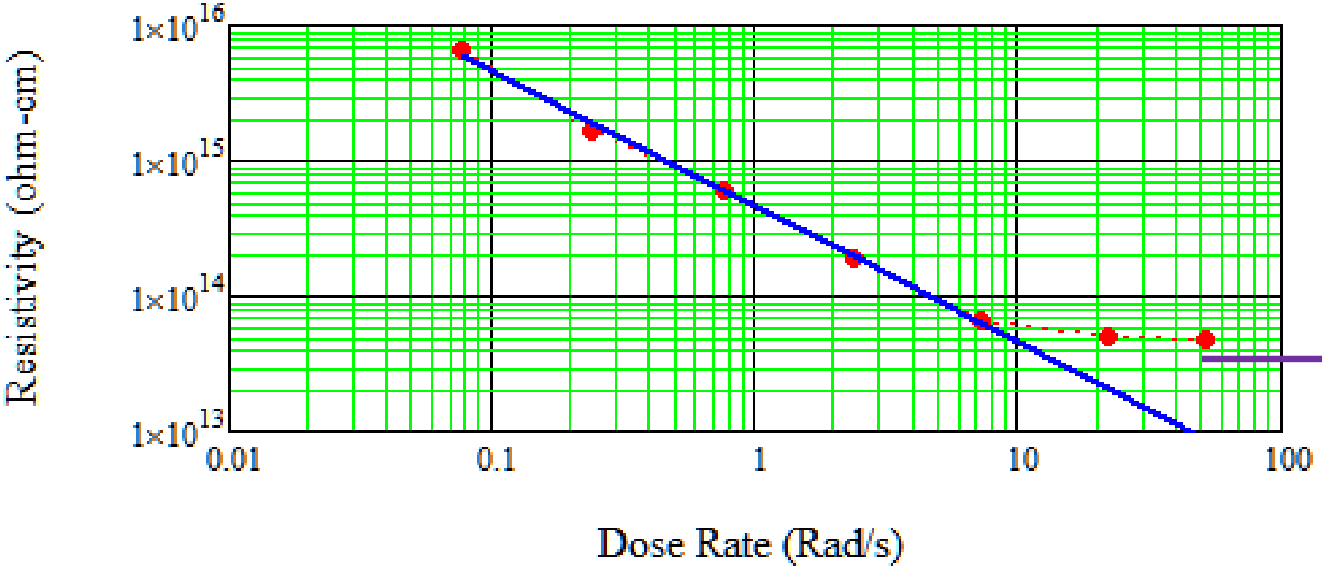

Fitting parameters
k_p = (2.0±0.3)10^{-15}(ohm-cm-rad/sec) $^{-1}$
Δ=1.01±0.03

Saturation for high dose rate

USU Materials Physics Group Capabilities

Facilities & Capabilities

Sample Characterization & Preparation

- Bulk composition (AA, IPC).
- Surface contamination (AES, AES mapping ESD).
- Surface morphology (SEM, optical microscopy).

Conduction Related Properties:

- Bulk & surface conductivity.
- High resistivity testing.
- Capacitance, dielectric constant, charge decay monitoring, and electrostatic discharge.

Electron Induced Emission:

- Total, secondary and backscattered yield vs. incident energy and angle.
- Energy-, angle-resolved emission spectra.
- Cathodoluminescence

Ion Induced Emission:

- Total electron and ion yield versus incident energy and angle.

Photon Induced Emission:

- Total electron yield vs photon energy.
- Energy-angle resolved photoelectron yield cross-sections.

Electron Induced Arcing:

- Four ultrahigh vacuum chambers for electron emission tests equipped with electron, ion, and photon sources, detectors, and surface analysis capabilities.
- Two high vacuum chambers for resistivity tests.
- High vacuum chamber for electrostatic breakdown tests.
- Ultrahigh vacuum chamber for pulsed electro acoustic measurements of internal charge distributions.

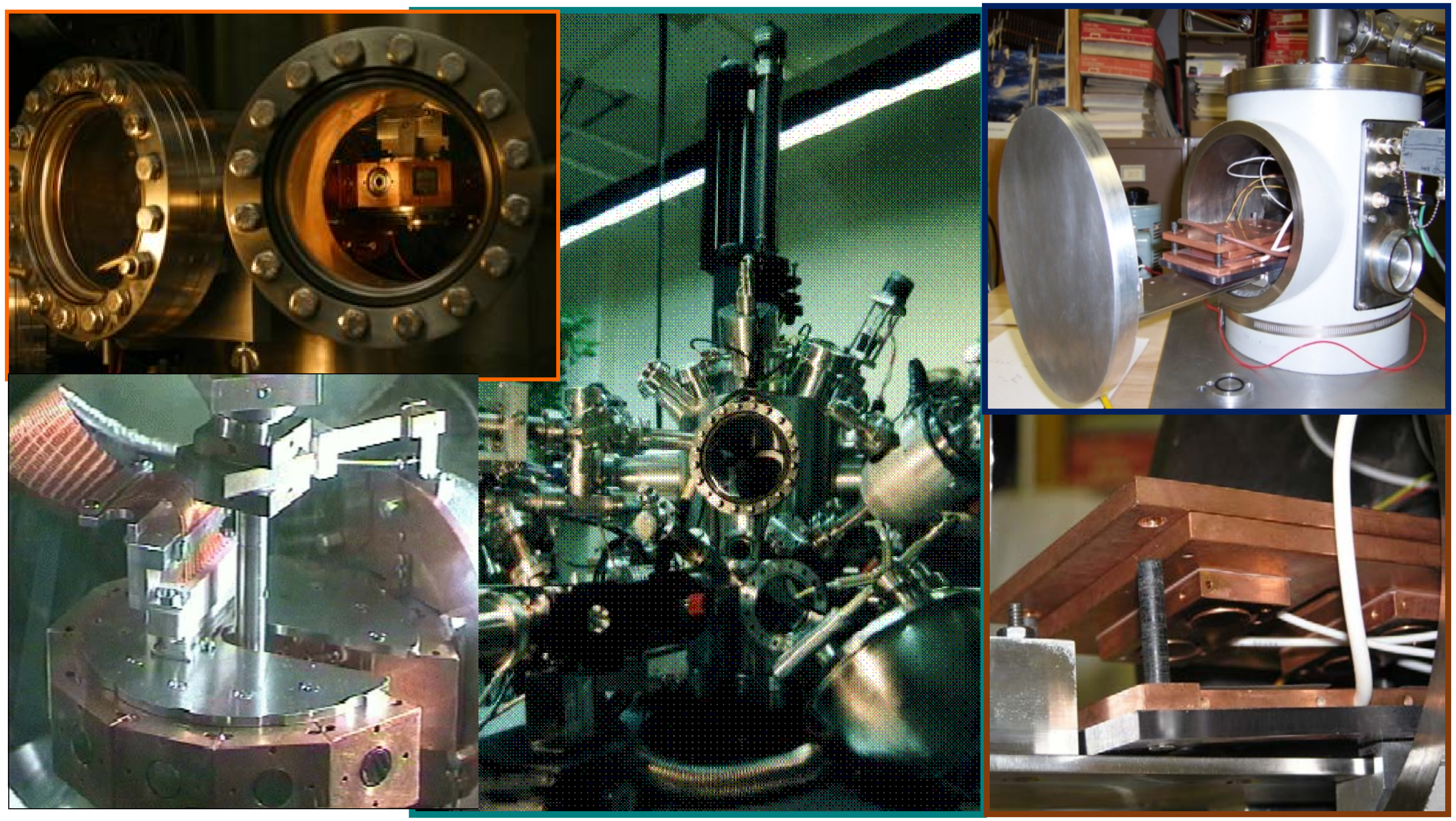

Dark Current and Radiation Induced Conductivites

Slab (parallel plate capacitor) Model

Charge Absorption

Bethe Approximation:

Charge absorbed at single (energy dependant) Range, R

Surface Potential

No Dissipation: $$V_S(t) = \frac{J_B R}{2\varepsilon_o \varepsilon_r} t$$

Dissipation:

$$V_S(t) = \frac{J_B R}{2\varepsilon_o \varepsilon_r} \left[\frac{1}{t} + \frac{2}{\tau_{DC}} + \frac{2}{\tau_{RIC}} \right]^{-1}$$

Decay Time: $$\tau_{DC} = \varepsilon_o \varepsilon_r / \sigma_{DC}$$

Energy Absorption

Continuous Slow Down Approximation:

Energy absorbed uniformly up to Range, R

Absorbed Dose Rate (J/kg-s):

Dose Rate: $$\dot{D} = J_B E_B / q_e \rho_m R$$

RIC: $$\sigma_{RIC}(\dot{D}) = k_{RIC} \cdot \dot{D}^{\Delta}$$

Decay Time: $$\tau_{RIC} = \varepsilon_o \varepsilon_r / \sigma_{RIC}$$

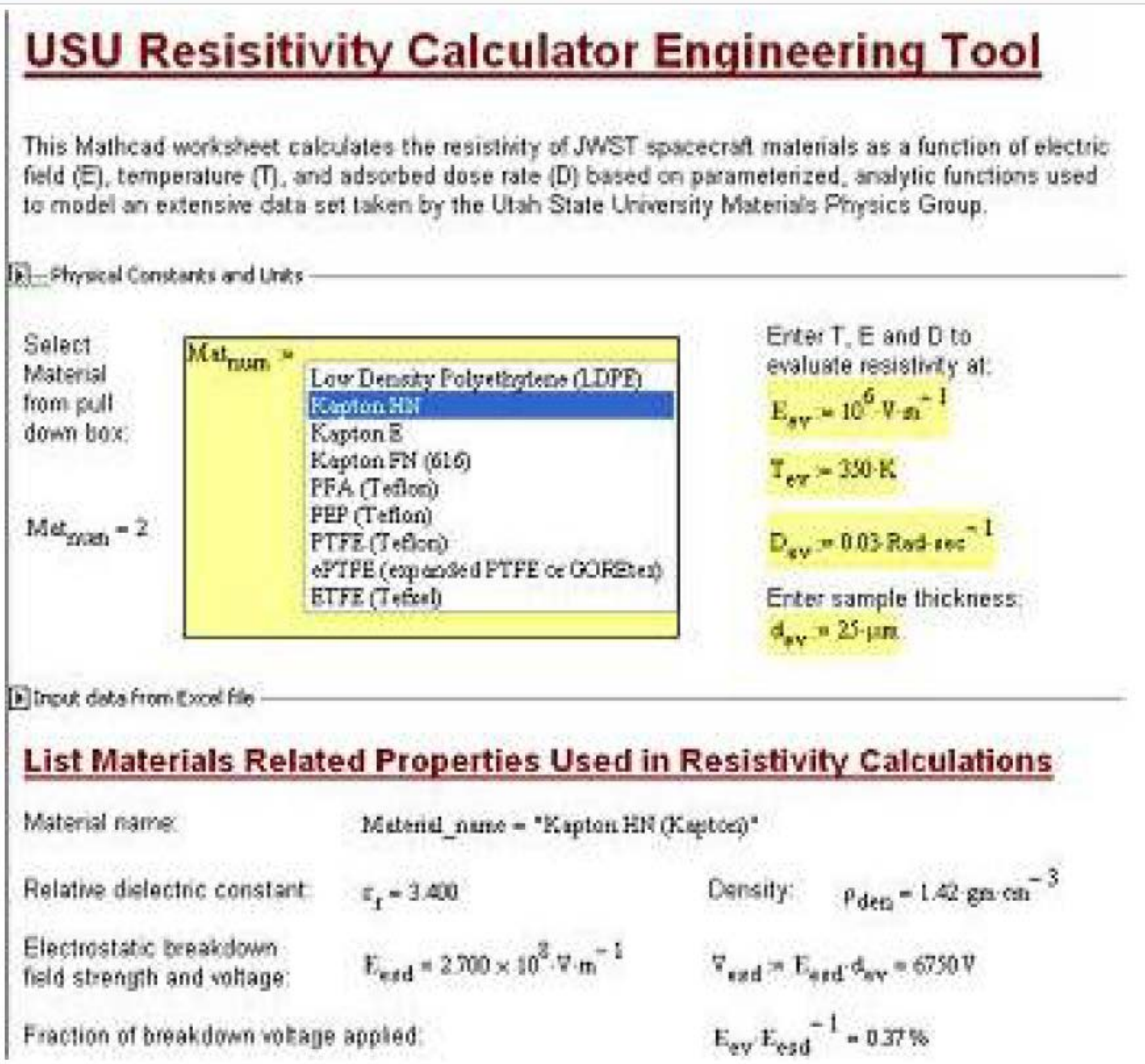

Figure 1. Mathcad engineering tool user input interface.

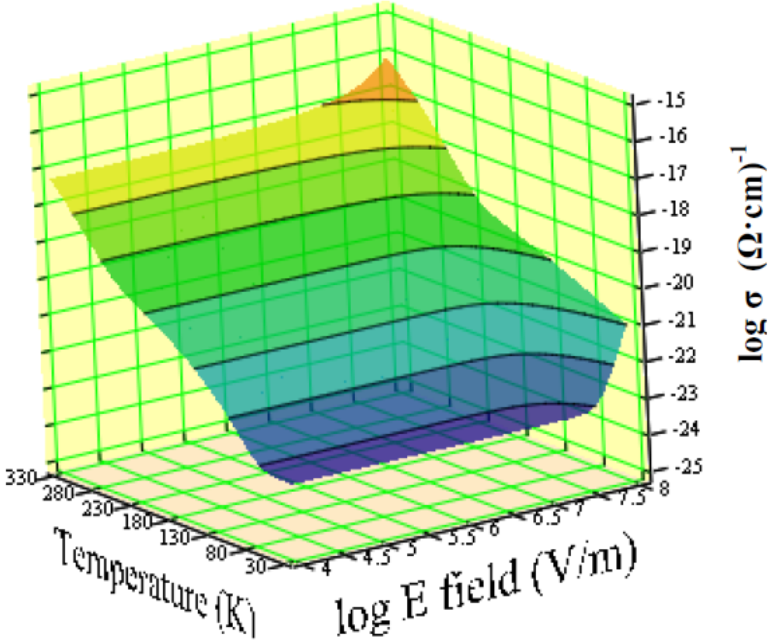

(a)

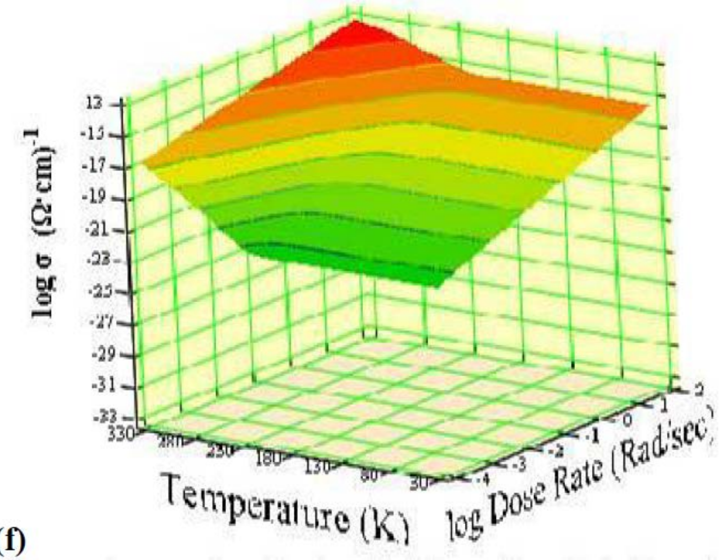

(f)

Conductivity in Highly Disordered Insulating Materials

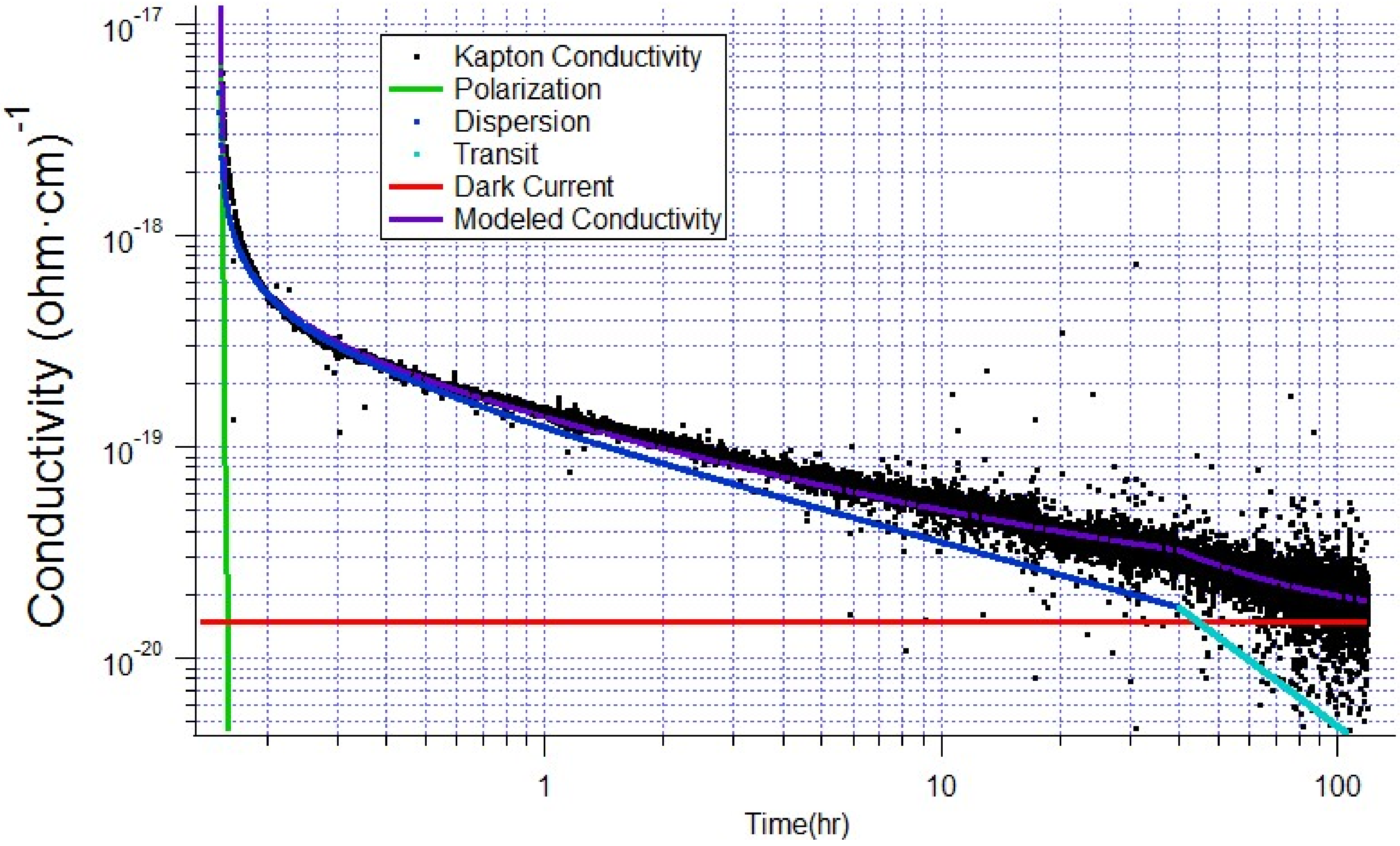

Kapton^{TM} (polyimide)

$$\sigma(t) = \sigma_{DC} + \sigma_{Polarization}(t) + \sigma_{Diffusion}(t) + \sigma_{Dispersion}(t) + \sigma_{Transit}(t) + \sigma_{RIC}(t)$$

Conductivity in HDIM--Polarization

$$\sigma(t) = \sigma_{DC} + \sigma_{Polarization}(t) + \sigma_{Diffusion}(t) + \sigma_{Dispersion}(t) + \sigma_{Transit}(t) + \sigma_{RIC}(t)$$

Polarization $\sigma^{o}_{Pol} e^{-t/\tau_{Pol}}$

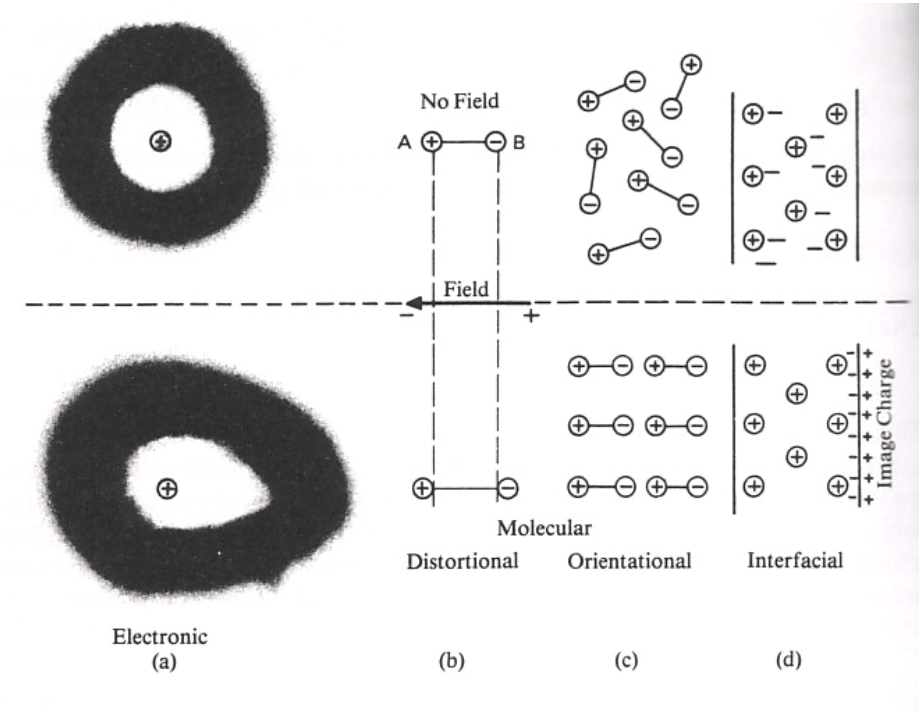

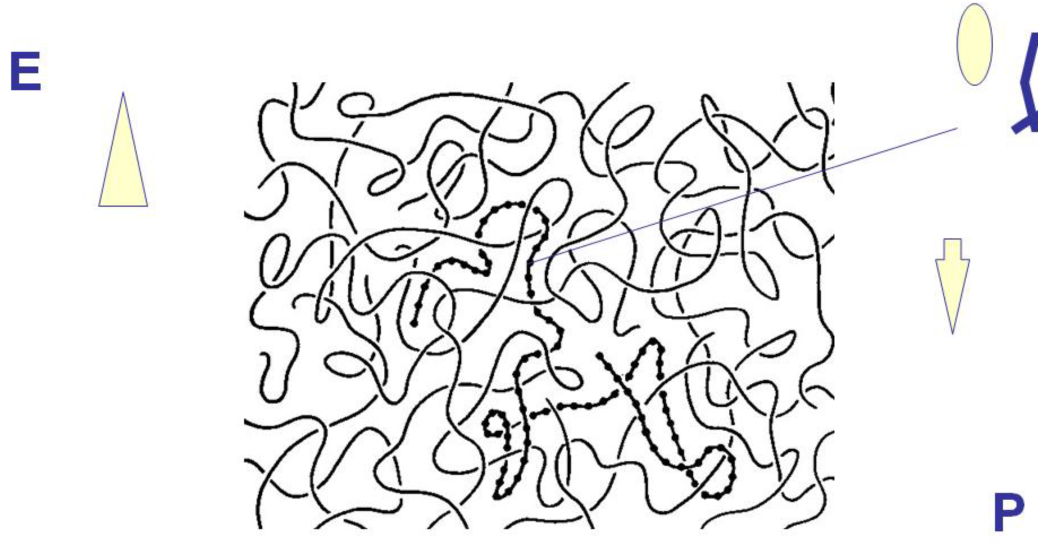

Conductivity in HDIM—Drift and Hopping Conduction

$$\sigma(t) = \sigma_{DC} + \sigma_{Polarization}(t) + \sigma_{Diffusion}(t) + \sigma_{Dispersion}(t) + \sigma_{Transit}(t) + \sigma_{RIC}(t)$$

$$\sigma^{o}_{Diff}\, t^{-1}$$

$$\sigma_{hop}(E,T) = \left[\frac{2 \cdot n(T) \cdot \nu \cdot a \quad \cdot e}{E}\right] \exp\left[\frac{-\Delta H}{k_B \cdot T}\right] \sinh\left[\frac{\varepsilon \cdot E \cdot a}{2 \cdot k_B \cdot T}\right]$$

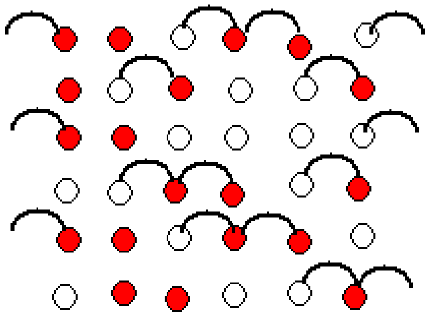

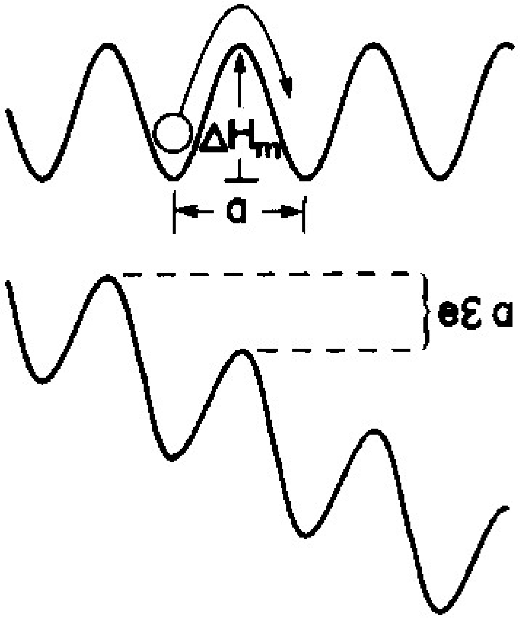

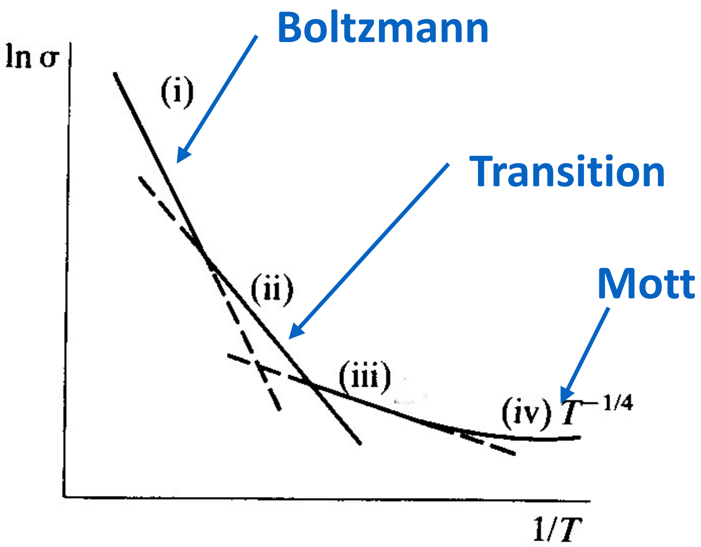

Temperature Dependence of Hopping Conductivity

At high temperatures, the conductivity is proportional to a Boltzmann factor, with trap depth ΔH:

$$\sigma(T) \propto \exp\left[-\frac{\Delta H}{k_B \cdot T}\right] \quad or \quad \rho(T) \propto \exp\left[\frac{\Delta H}{k_B \cdot T}\right]$$

At low temperatures, the variable-range hopping conductivity is proportional to a Mott factor:

$$\sigma(T) \propto \exp\left[-\frac{1}{k_B \cdot T^{1/4}}\right] \quad or \quad \rho(T) \propto \exp\left[\frac{1}{k_B \cdot T^{1/4}}\right]$$

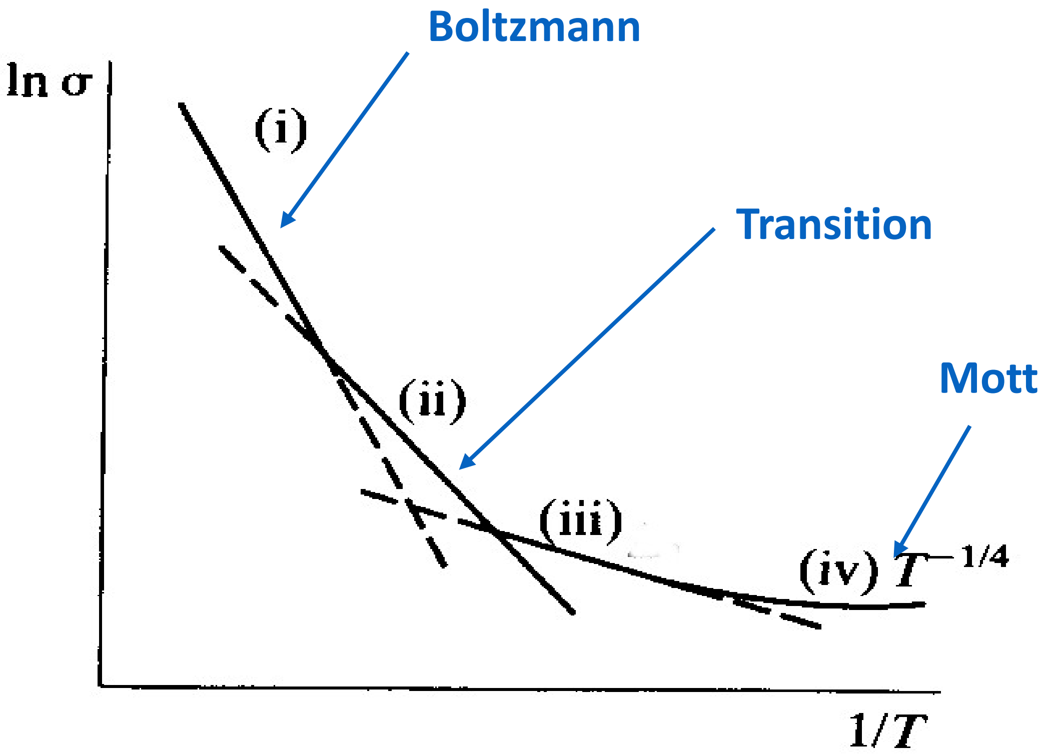

Conductivity in HDIM—E-Field Dependence of Hopping Conductivity

At low field, the conductivity is independent of E-field:

$$\rho_{hop}(T) \xrightarrow{low\,E} \left[\frac{n(T)\cdot \nu \cdot a^2 \cdot e^2}{k_B \cdot T}\right]^{-1} \exp\left[\frac{\Delta H}{k_B \cdot T}\right]$$

At high field, the potential wells distort. Poole-Frenkle theory predicts:

$$\rho(E;T) = \rho_o(T)\exp\left[-\frac{\beta\ \mathrm{E}^{0.5}}{k_B \cdot T}\right]$$

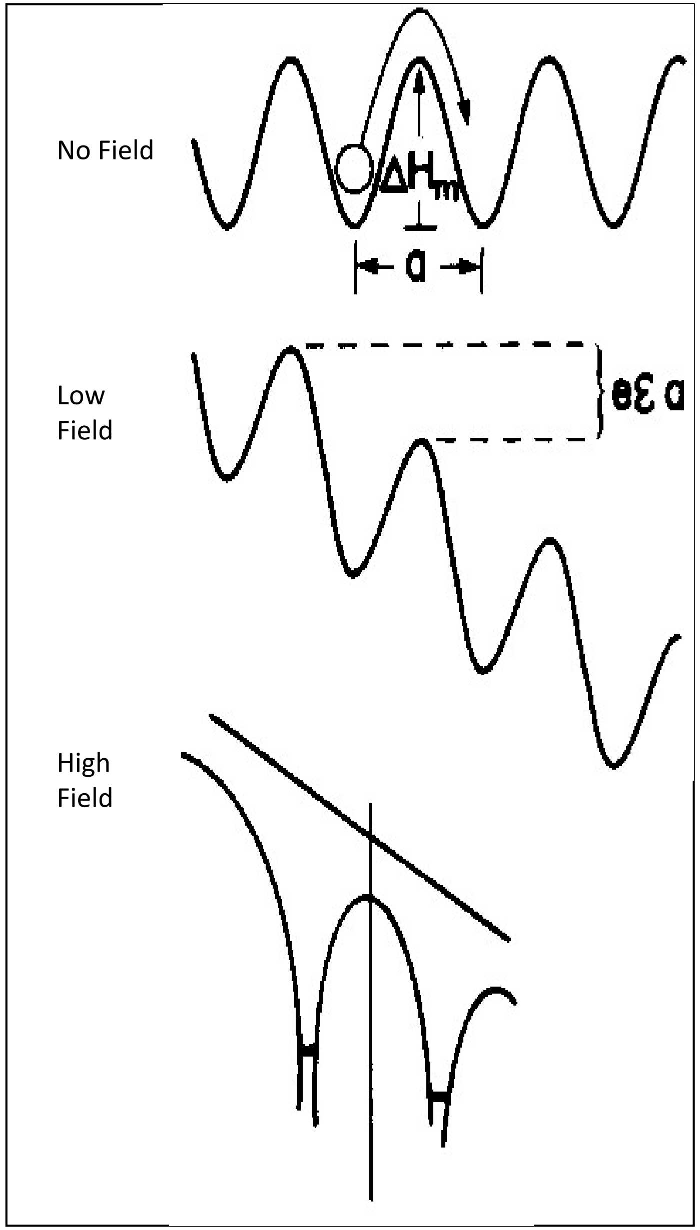

Diffusive and Dispersive Transport

$$\sigma(t) = \sigma_{DC} + \sigma_{Polarization}(t) + \sigma_{Diffusion}(t) + \sigma_{Dispersion}(t) + \sigma_{Transit}(t) + \sigma_{RIC}(t)$$

$$\sigma^{o}_{Disp}\, t^{-(1-\alpha)} + \sigma^{o}_{Trans}\, t^{-(1+\alpha)}$$

$$I(t) \sim \begin{cases} t^{-(1-\alpha)}, & t < t_T \\ t^{-(1+\alpha)}, & t > t_T \end{cases}$$

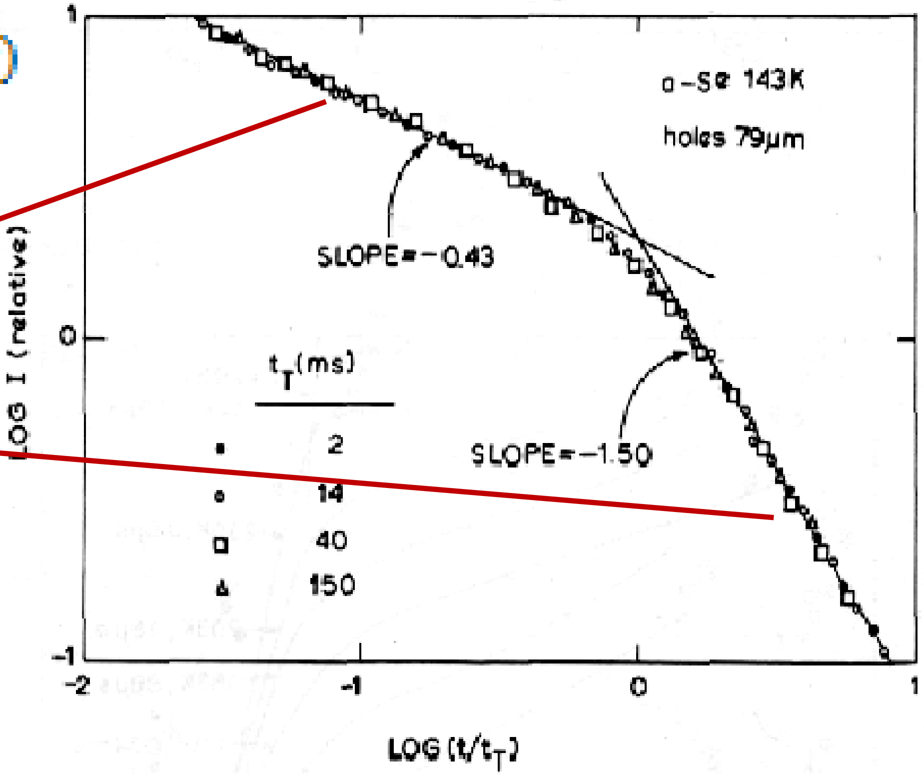

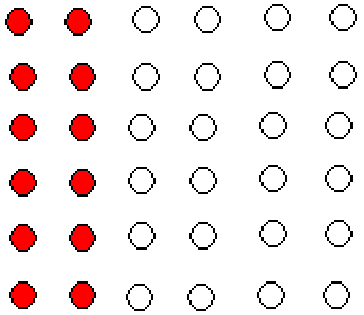

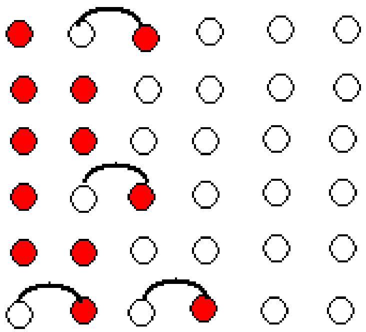

- Photoconductivity experiment on semiconductors by Pfister and Sherr
- Amorphous Selenium
- Dispersive transport causes unique shape in log-log graph
- Hopping and trapping mechanisms responsible for dispersive transport
- Dispersive transport results from wide range of hopping times, e.g. from range of *ΔH* and *a*
- 'Universality' a result of dispersive transport
- Note transit times in ms

Normal vs. Dispersive Transport

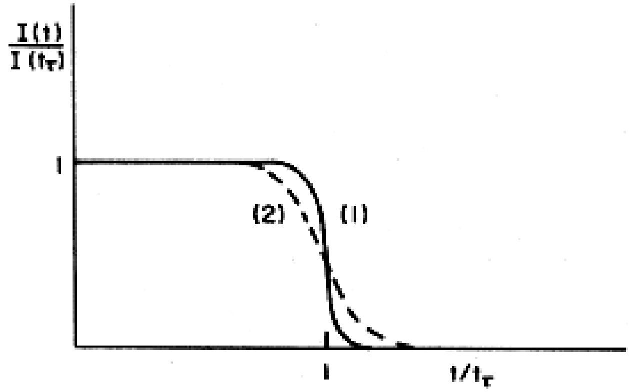

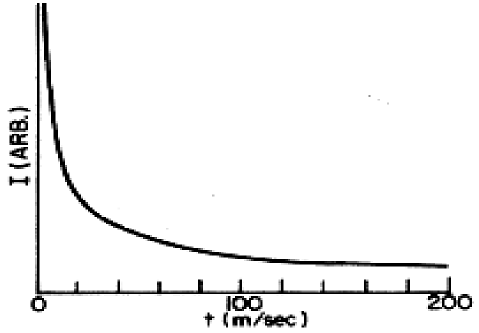

I/t Curves

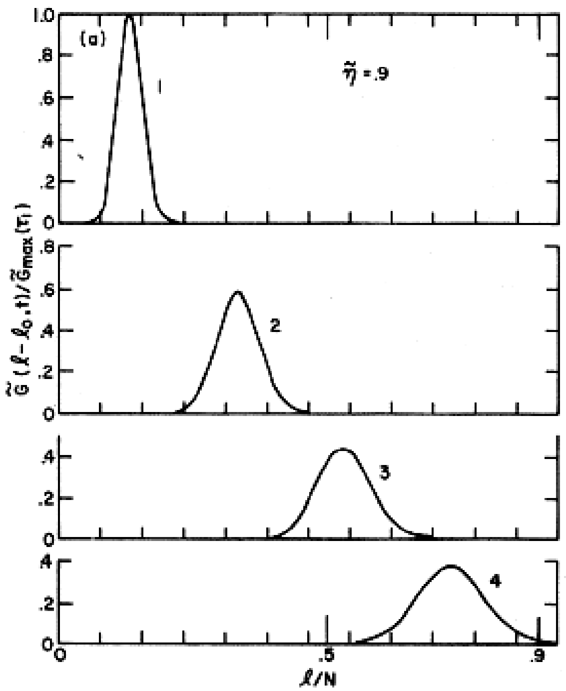

Pulse Propagation

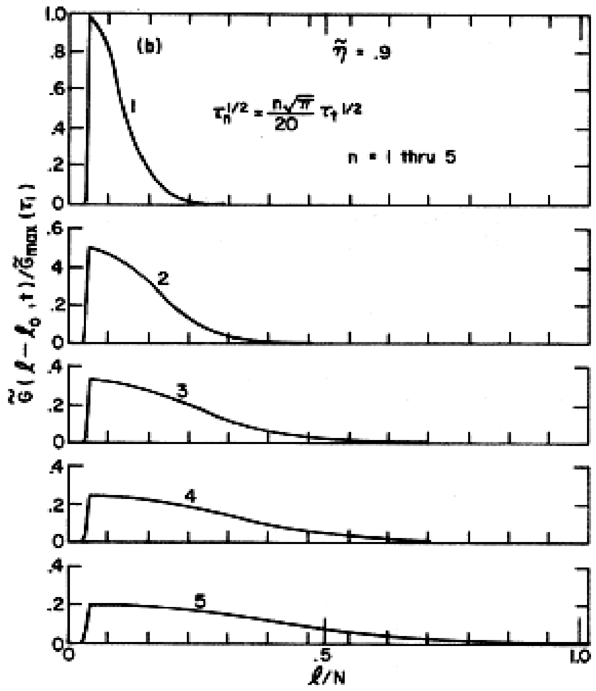

H. Scher and E.W. Montroll, Anomalous transit-time dispersion in amorphous solids, Phys. Rev. B, 1975

Theory

RIC and Defect Density of States

A Materials Physics Approach to the Problem

Measurements with many methods…

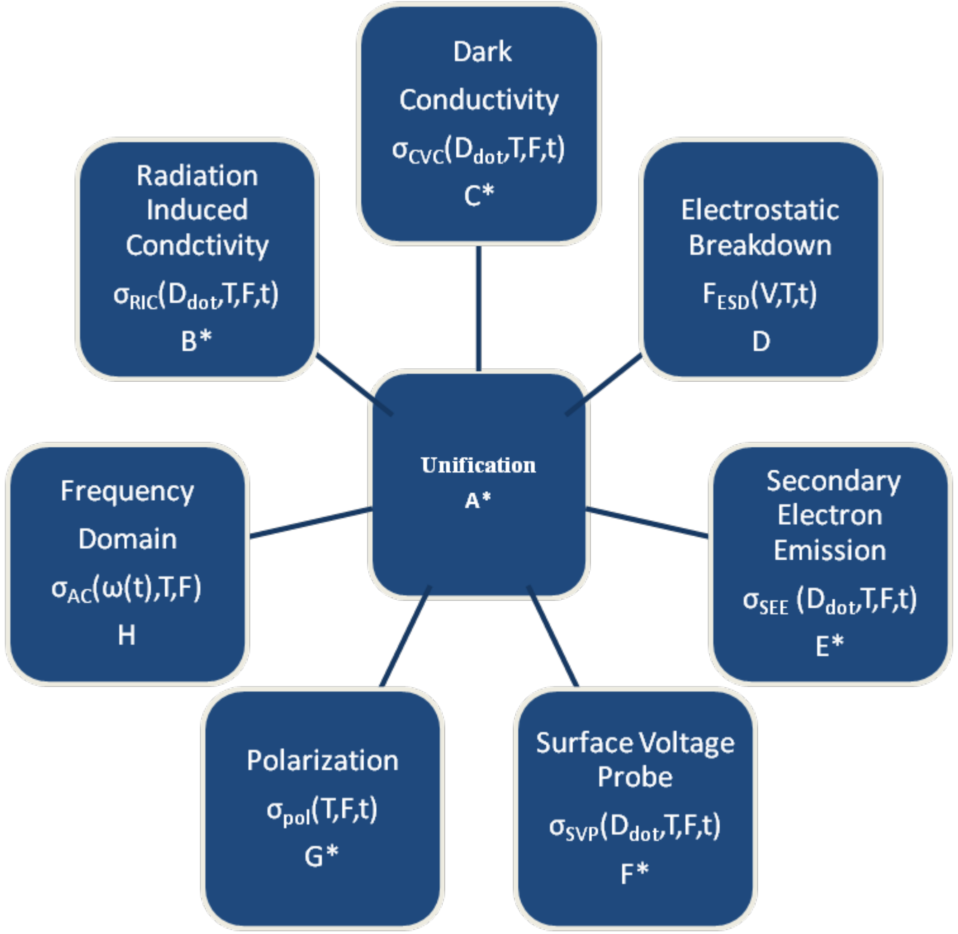

Interrelated through a…

Complete set of dynamic transport equations

$$J = q_e n_e(z,t)\mu_e F(z,t) + q_e D \frac{dn_{tot}(z,t)}{dz}$$

$$\frac{\partial}{\partial z} F(z,t) = q_e n_{tot} / \epsilon_0 \epsilon_r$$

$$\frac{\partial n_{tot}(z,t)}{\partial t} - \mu_e \frac{\partial}{\partial z}[n_e(z,t)F(z,t)] - q_e D \frac{\partial^2 n_e(z,t)}{\partial z^2} = N_{ex} -$$

$$\alpha_{er}\, n_e(z,t) n_{tot}(z,t) + \alpha_{et}\, n_e(t)[N_t(z) - n_t(z,t)]$$

$$\frac{dn_h(z.t)}{dt} = N_{ex} - \alpha_{er}\, n_e(z,t) n_h(z,t)$$

$$\frac{dn_t(z,\varepsilon,t)}{dt} = \alpha_{et} n_e(z,t)[N_t(z,\varepsilon) - n_t(z,\varepsilon,t)] -$$

$$\alpha_{te} N_e exp\left[-\frac{\varepsilon}{kT}\right] n_t(z,\varepsilon,t)$$

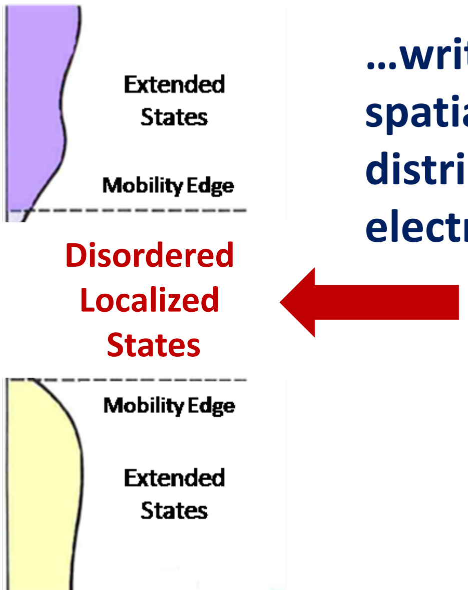

…written it terms of spatial and energy distribution of electron trap states

A Focus on Defect Densities

What is required is knowledge of:

- **Defect (trap) spatial distribution (density)**
- **Defect energy distribution (DOS)**
- **Types of charge carriers (*e.g.*, e$^-$ or h$^+$)**
- **Occupation of defect states by charge carriers**
- **Transition frequencies (lifetimes)**
- **Complete set of dynamic transport equations**

$$J = q_e n_e(z,t)\mu_e F(z,t) + q_e D \frac{dn_{tot}(z,t)}{dz}$$

$$\frac{\partial}{\partial z} F(z,t) = q_e n_{tot}/\epsilon_0 \epsilon_r$$

$$\frac{\partial n_{tot}(z,t)}{\partial t} - \mu_e \frac{\partial}{\partial z}[n_e(z,t)F(z,t)] - q_e D \frac{\partial^2 n_e(z,t)}{\partial z^2} = N_{ex} - \alpha_{er}\, n_e(z,t) n_{tot}(z,t) + \alpha_{et}\, n_e(t)[N_t(z) - n_t(z,t)]$$

$$\frac{dn_h(z.t)}{dt} = N_{ex} - \alpha_{er}\, n_e(z,t) n_h(z,t)$$

$$\frac{dn_t(z,\varepsilon,t)}{dt} = \alpha_{et} n_e(z,t)[N_t(z,\varepsilon) - n_t(z,\varepsilon,t)] - \alpha_{te} N_e exp\left[-\frac{\varepsilon}{kT}\right] n_t(z,\varepsilon,t)$$

Disorder introduces localized states in the gap

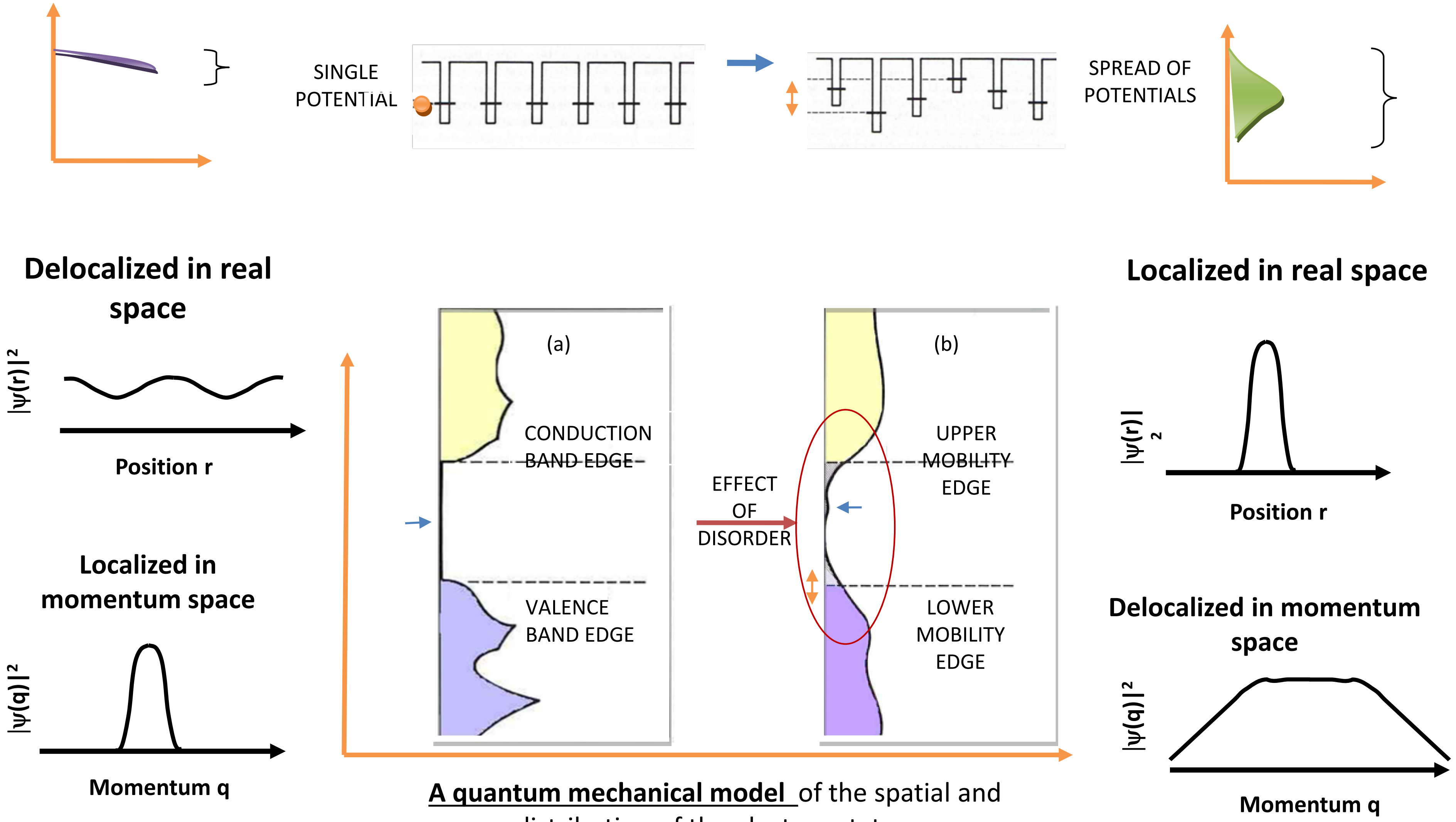

A quantum mechanical model of the spatial and energy distribution of the electron states

Nobel Prize 1977 to Sir Nevill Mott and P.W. Anderson, *Electronic Structure of Disordered Systems*

Tunneling Between Traps—and Mott Anderson Transitions

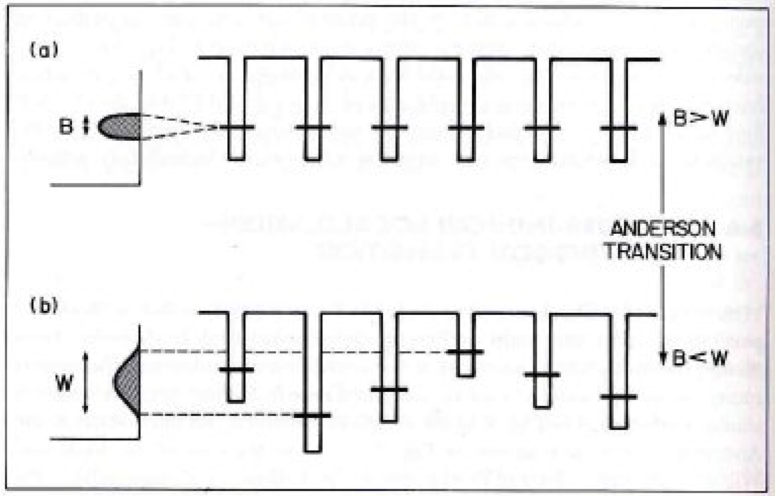

Figure 5.13 One-electron tight-binding picture for the Anderson transition. When the width W of the disorder exceeds the overlap bandwidth B, disorder-induced localization takes place.

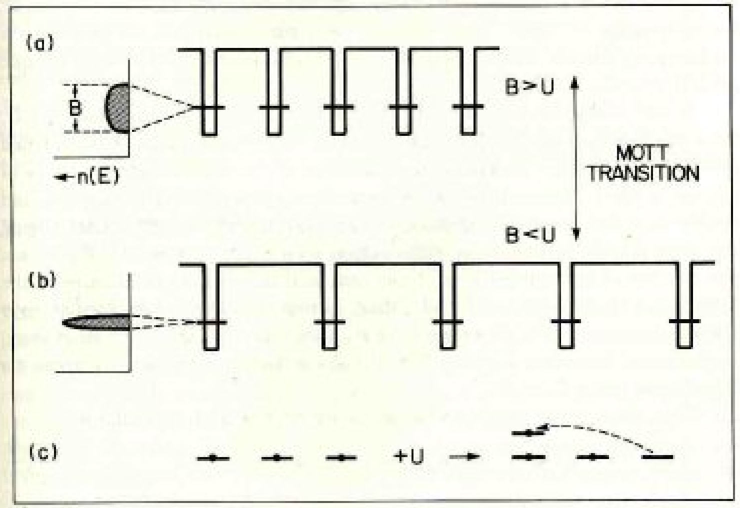

Figure 5.12 Schematic picture for the Mott transition. When the electron bandwidth B is decreased (by increased atom–atom separation) sufficiently to be smaller than the intrasite electron–electron energy U, correlation-induced localization takes place.

Anderson transition between extended Bloch states and localized states caused by variations in well depth affects tunneling between states.

Mott transition between extended Bloch states and localized states caused by variations in well spacing which affects tunneling between states.

R. Zallen, *The Physics of Amorphous Solids*, (John Wiley and Sons, Inc. 1983).

Nobel Prize 1977 to Sir Neville Mott and P.W. Anderson*, Electronic Structure of Disordered Systems*

Synergistic Models of Electron Emission and Transport Measurements of Disordered SiO_2

Look at measurements of fused quartz (a-SiO_2) from a synergistic microscopic, defect state perspective

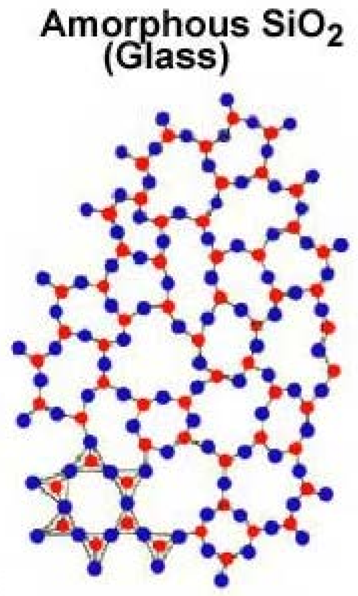

used as coverglass, optical elements, and insulator

Putting the Pieces Together

Focus on DOS:

- Synthesis of results from different studies and techniques

- Development of overarching theoretical models allow extension of measurements made over limited ranges of environmental parameters to make predictions for broader ranges encountered in space.

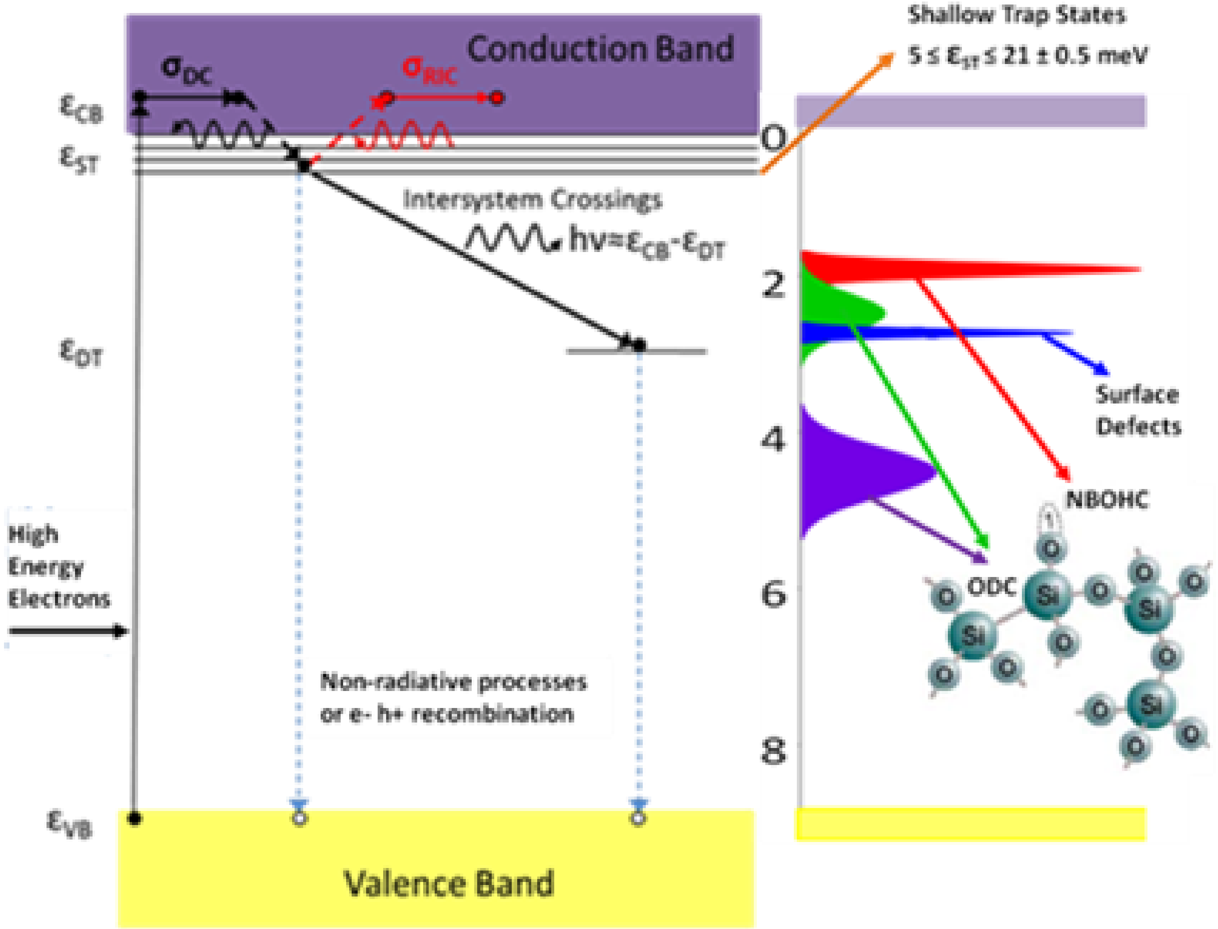

Band	Peak	Peak	FWHM	Defect	Ref.
Red	1.93±0.01 eV	663±3 nm	42 nm	NBOHC	[16,20,23]
Green	2.48±0.03	506±7	68	ODC	[17,23]
Blue	2.76±0.03	450±5	11	Surface	[18-20,23]
UV	4.97	275	50	ODC	[17-20,23]

Optical Band Gap—Disordered SiO_2

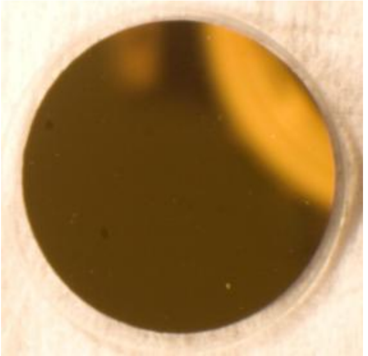

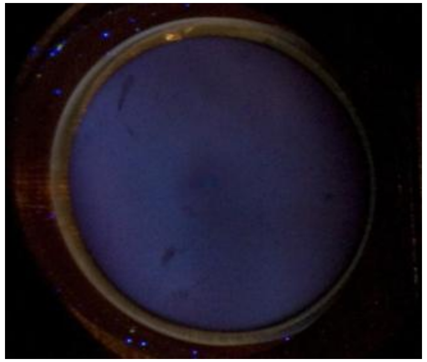

Optical Transmission Data:
- **Direct band gap ~8.9 eV**
- **Additional steps in transmission in 1-4 eV range**

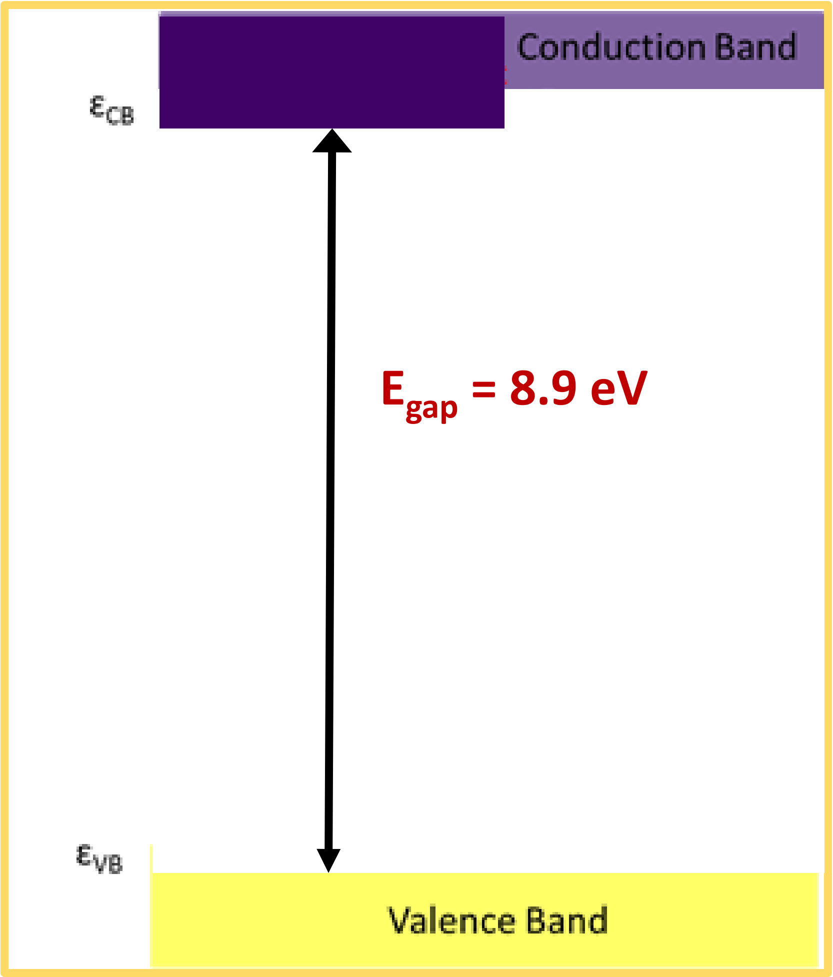

Conductivity vs Temperature

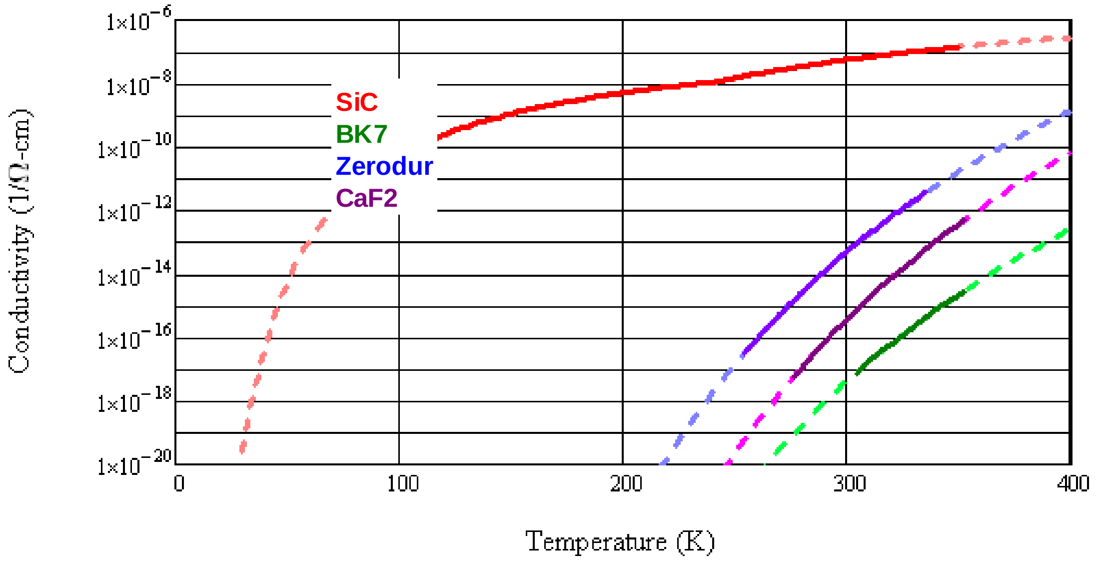

$$\sigma_{hop}(E,T) = \left[\frac{2 \cdot n(T) \cdot \nu \cdot a \quad \cdot e}{E}\right] \exp\left[\frac{-\Delta H}{k_B \cdot T}\right] \sinh\left[\frac{\varepsilon \cdot E \cdot a}{2 \cdot k_B \cdot T}\right]$$

Yields:

Defect energy, E_d
and
Trap density, N_T

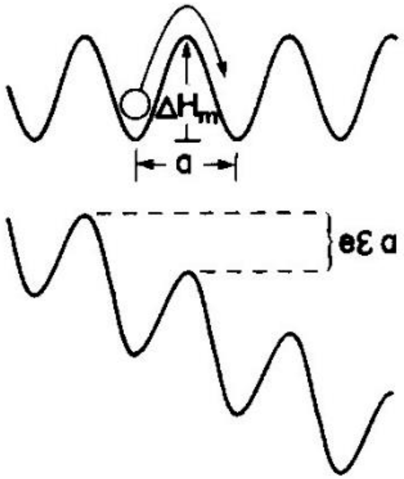

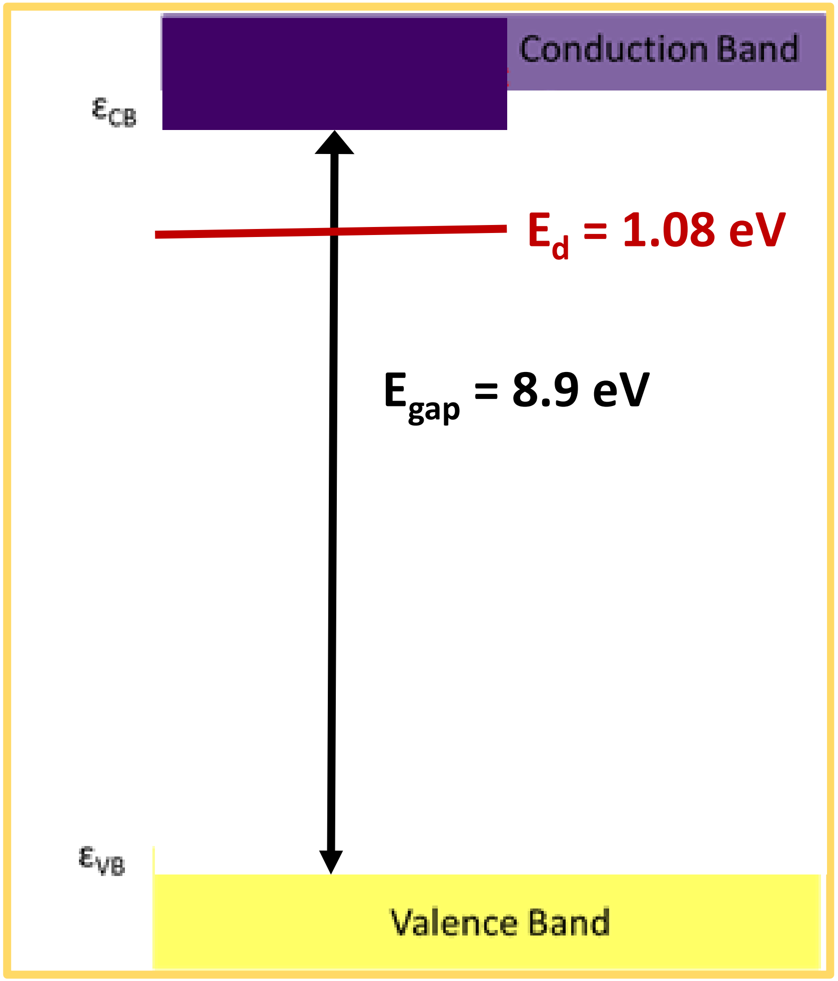

Conductivity Modes vs Time

$$\sigma(t)=\sigma_{DC}\left[1+\frac{\sigma_{AC}(\nu)}{\sigma_{DC}}+\frac{\sigma^{o}_{pol}}{\sigma_{DC}}e^{\frac{-t}{\tau_{pol}}}+\frac{\sigma^{o}_{diffusion}}{\sigma_{DC}}t^{-1}+\frac{\sigma^{o}_{dispersive}}{\sigma_{DC}}t^{-(1-\alpha)}+\frac{\sigma^{o}_{transit}}{\sigma_{DC}}t^{-(1+\alpha)}+\frac{\sigma^{o}_{RIC}}{\sigma_{DC}}\left(1-e^{-\tau^{1}_{RIC}/(t-t_{on})}\right)\left(1+\left(t-t_{off}\right)/\tau^{2}_{RIC}\right)^{-1}\right]$$

Dark Current · AC · Polarization · Diffusion · Pre-Transit · Post-Transit · RIC · RIC Rise · Persistent RIC

- **Dark current or drift conduction—Defect density, N_T, and $E_d \approx 1.08$ eV**
- **Diffusion-like and dispersive conductivity—Energy width of trap distribution, α**
- **Radiation induced conductivity—Shallow trap density and ε_{ST}**
- **Polarization—Rearrangement of bound charge, $\epsilon_r^{\infty}\epsilon_o$ and τ_{pol}**
- **AC conduction—Dielectric response, $\epsilon_r(\nu)\epsilon_o$**

Surface Voltage Charging and Discharging

- Uses pulsed non-penetrating electron beam injection with no bias electrode injection.
- Fits to exclude AC, polarization, transit and RIC conduction.
- **Yields N_T, E_d, α, ε_{ST}**

Instrumentation

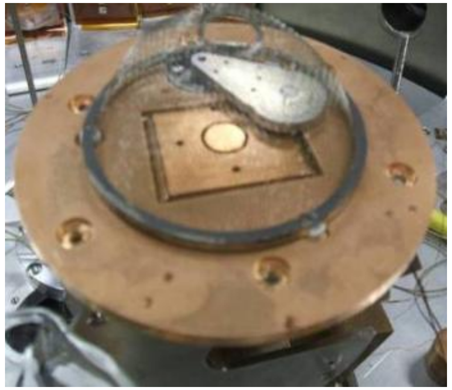

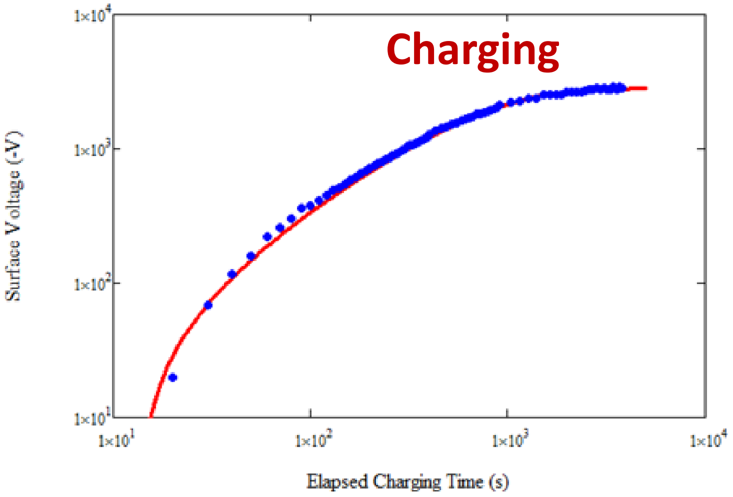

$$\sigma(t)=\sigma_o\left\{1+\left[\frac{\sigma^o_{diffusion}}{\sigma_o}\right]t^{-1}+\left[\frac{\sigma^o_{dispersive}}{\sigma_o}\right]t^{-(1-\alpha)}\right\}$$

Charging

$$V_s(t)=\frac{\left[\frac{q_e n_t^{max}}{\varepsilon_o\varepsilon_r}[1-Y(E_b)]\right]\left[R(E_b)D\left(1-\frac{R(E_b)}{2D}\right)\right]\left[\frac{\tau_Q}{t}\right]\left[1-e^{-\left(\frac{t}{\tau_Q}\right)\left\{1+\left(\frac{t\,\sigma_o}{\varepsilon_o\varepsilon_r}\right)\left[1+\frac{\sigma^o_{diffusion}}{\sigma_o}(t^{-1})+\frac{\sigma^o_{dispersive}}{\sigma_o}(t^{-(1-\alpha)})\right]\right\}^{-1}}\right]}{\left\{1+\left(\frac{t\,\sigma_o}{\varepsilon_o\varepsilon_r}\right)\cdot\left[1+\frac{\sigma^o_{diffusion}}{\sigma_o}(t^{-1})+\frac{\sigma^o_{dispersive}}{\sigma_o}(t^{-(1-\alpha)})\right]\right\}}$$

Discharge

$$V(t)=V_o\,e^{-t\sigma(t)/\epsilon_o\epsilon_r}$$

$$\approx V_o\left[1-\left(\frac{\sigma_o\,t}{\epsilon_o\epsilon_r}\right)\left\{1+\left[\frac{\sigma^o_{diffusion}}{\sigma_o}\right]t^{-1}+\left[\frac{\sigma^o_{dispersive}}{\sigma_o}\right]t^{-(1-\alpha)}\right\}\right]$$

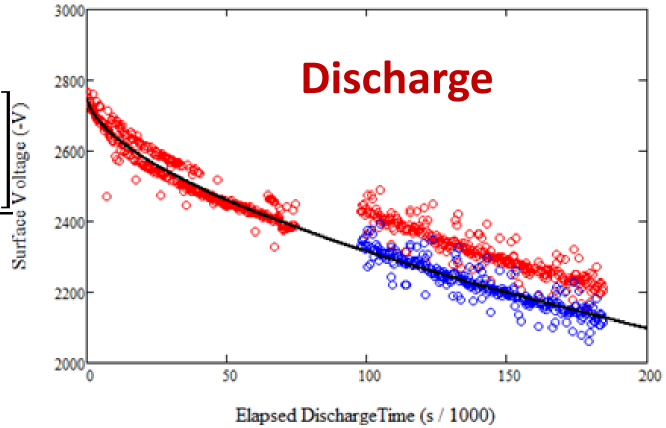

F_{ESD} Breakdown: Dual (Shallow and Deep) Defect Model

Yields:

Ratio of Defect energy to Trap density, $\Delta G_{def}/N_T$

Separate these with T dependence

ΔG_{def} =0.97 eV
N_T=1·10^{17} cm^{-3}

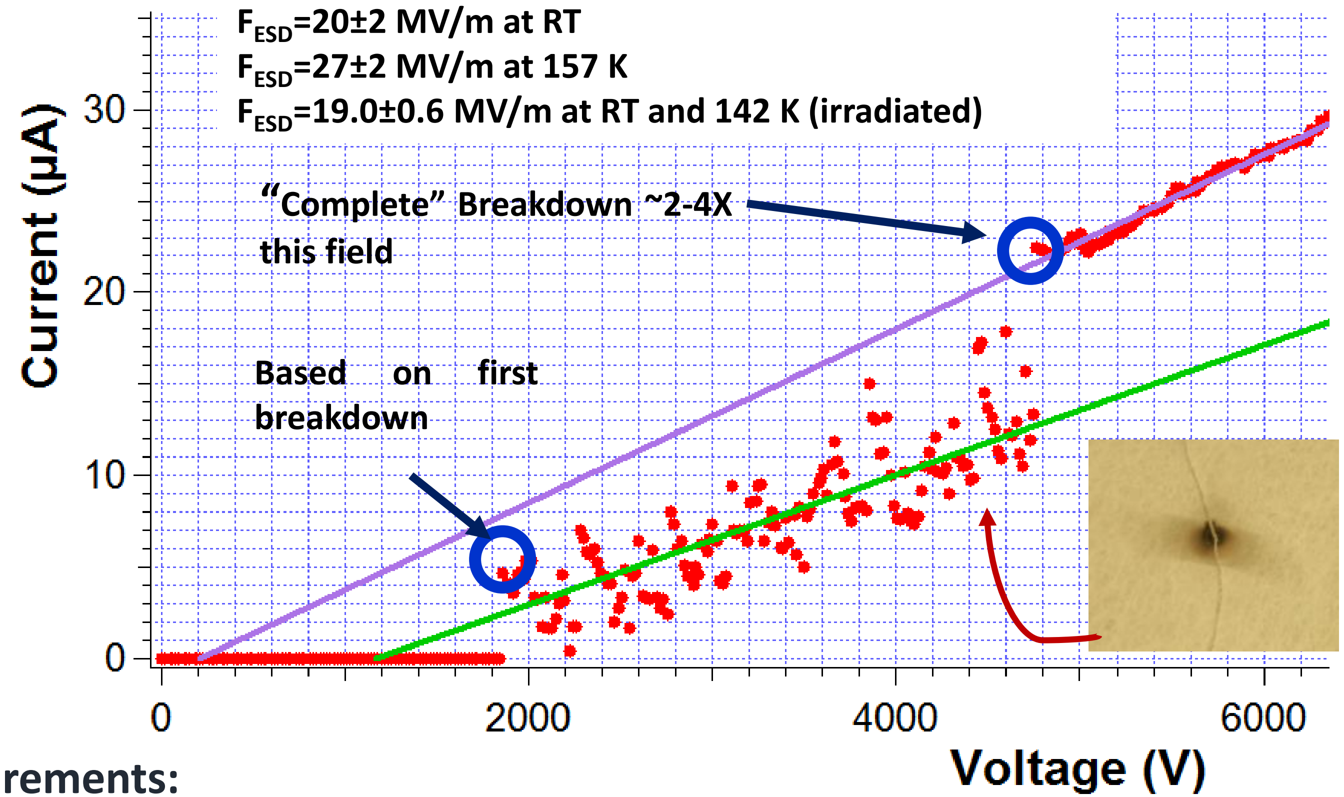

Breakdown field measurements:

$$N_{def}\ \Delta G_{def} = \frac{\varepsilon_0 \varepsilon_r}{2} \cdot (F_{ESD})^2$$

Endurance time measurements:

$$t_{en}(F,T) = \left(\frac{h}{2k_b T}\right) \exp\left[\frac{\Delta G_{def}(F,T)}{k_b T}\right] \operatorname{csch}\left[\frac{F^2 \varepsilon_0 \varepsilon_r}{2k_B T\ N_{def}(F,T)}\right]$$

RIC T-Dependence

Shallow Trap DOS Profile

Exponential DOS Below E_c

Effective Fermi Level

E_F^{eff} = 24 meV

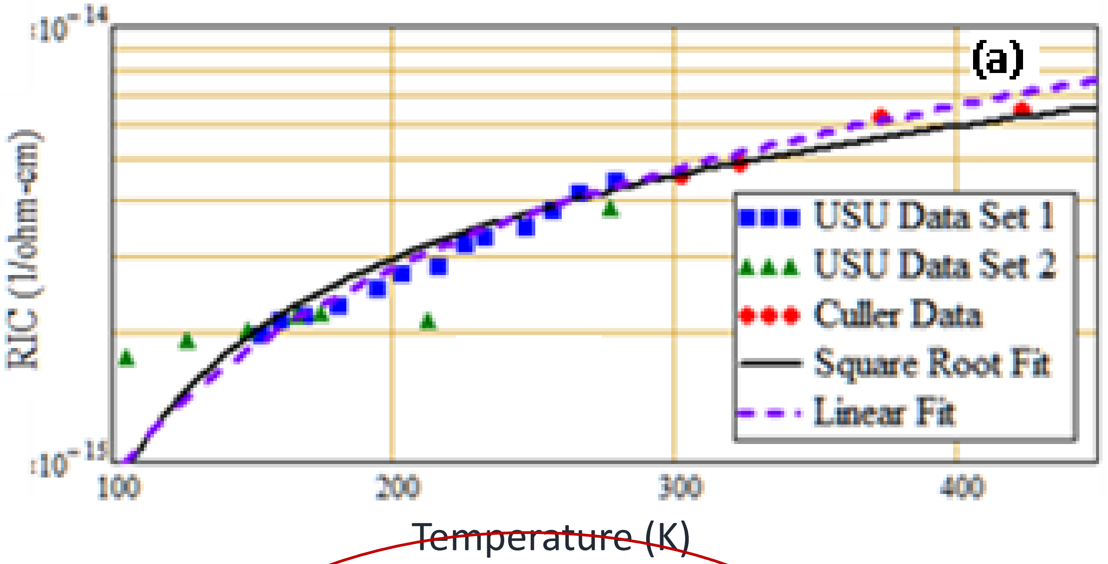

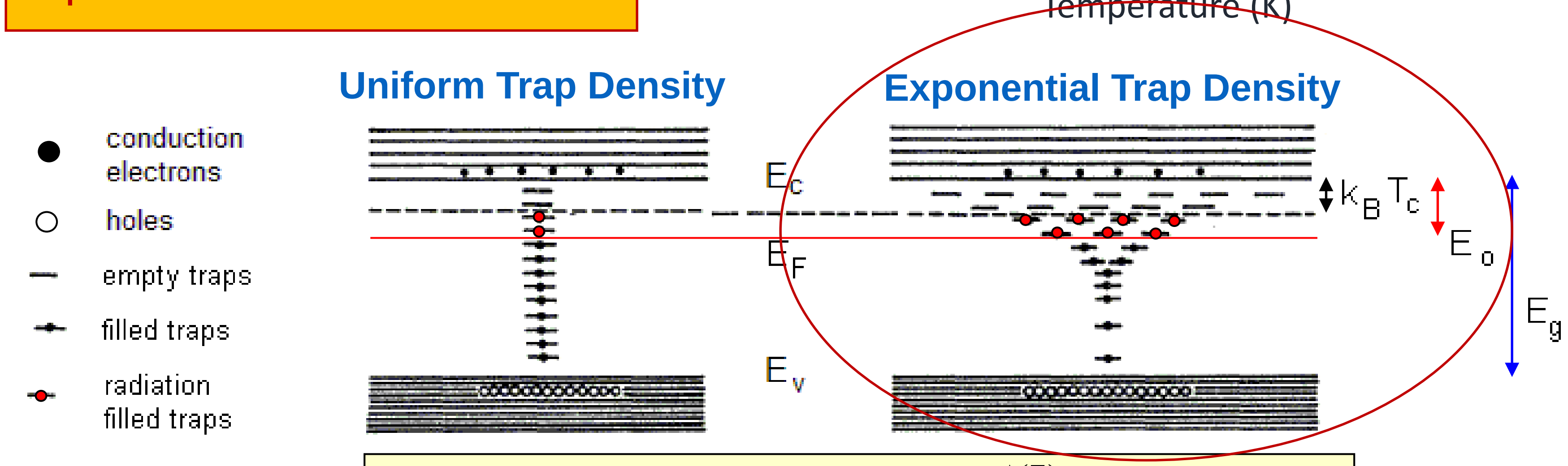

$$\sigma_{RIC}(T,D) = k_{RIC}(T) \cdot D^{\Delta(T)}$$

$$\Delta(T) \to 1 \qquad \qquad \Delta(T) \to T_c / (T + T_c)$$

$$k(T) \to k_{RICo} \qquad \qquad k(T) \to k_{RIC1}\left[2\left(\frac{m_e k_B T}{2\pi\hbar^2}\right)^{3/2}\left(\frac{m_e^* m_h^*}{m_e\, m_e}\right)^{3/4}\right]^{\frac{T}{T+T_c}}$$

Complementary Responses to Radiation: RIC and CL

Modified Joblonski band diagram

- VB electrons excited into CB by the high energy incident electron radiation.
- They relax into shallow trap (ST) states, then thermalize into lower available long-lived ST.

- Four paths are possible:

(i) Remain in (short lived) shallow traps
(ii) Non-radiative transitions or e^{-}-h^{+} recombination into VB holes;
(iii) Radiation induced conductivity (RIC), with thermal re-excitation into the CB or;
(iv) Relaxation to deep traps (DT), with concomitant photon emission.

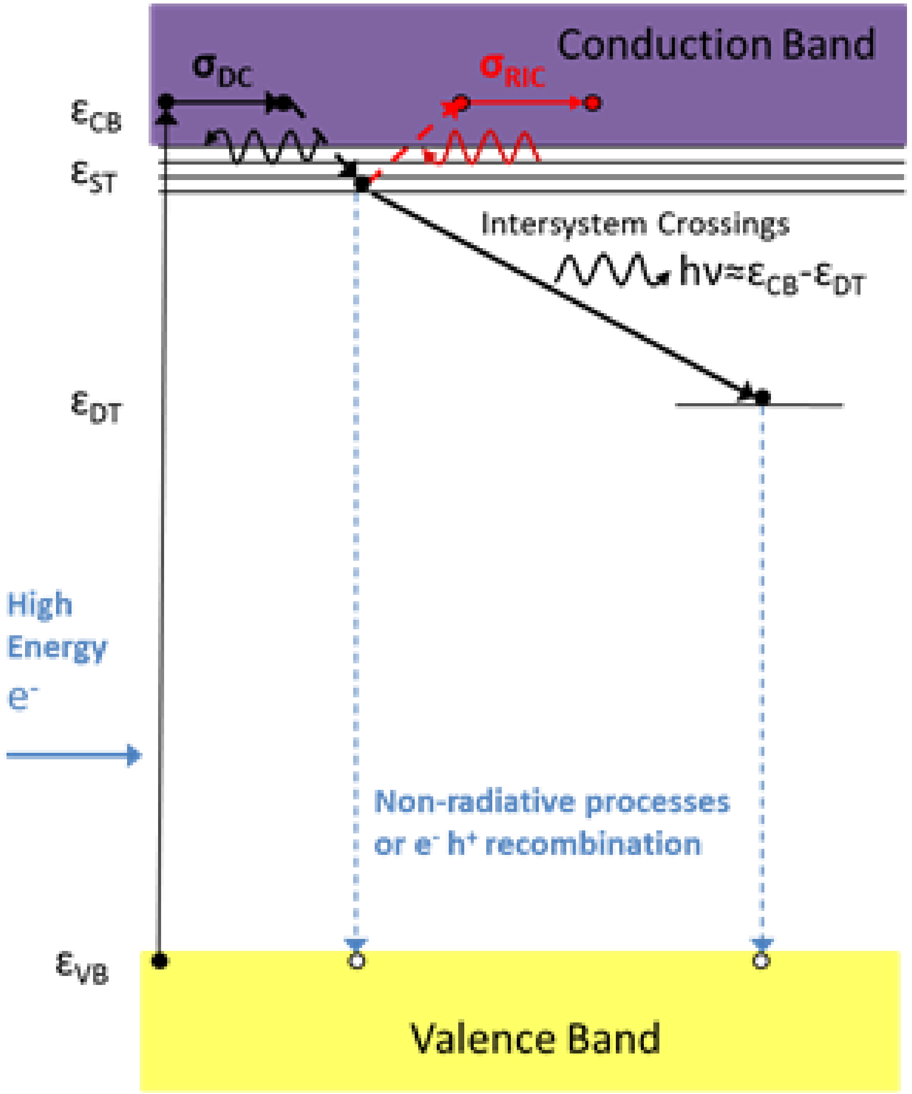

Cathodoluminescence Emission Spectra

Photon Emission Spectra
Peak Wavelength

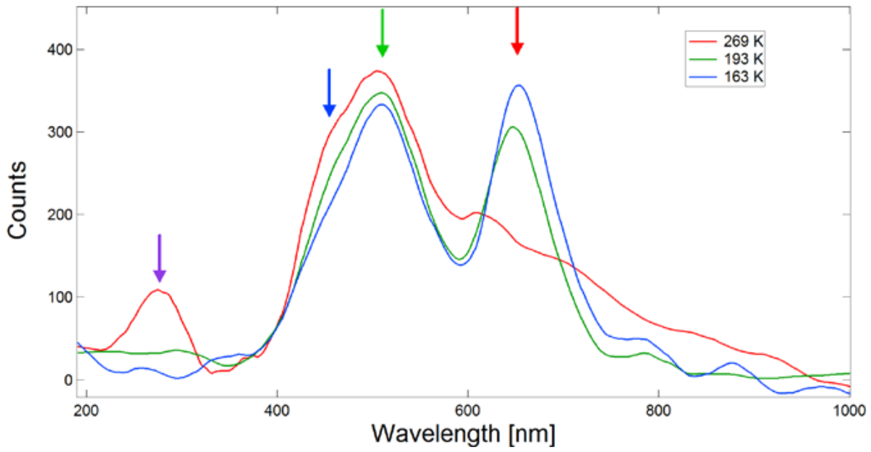

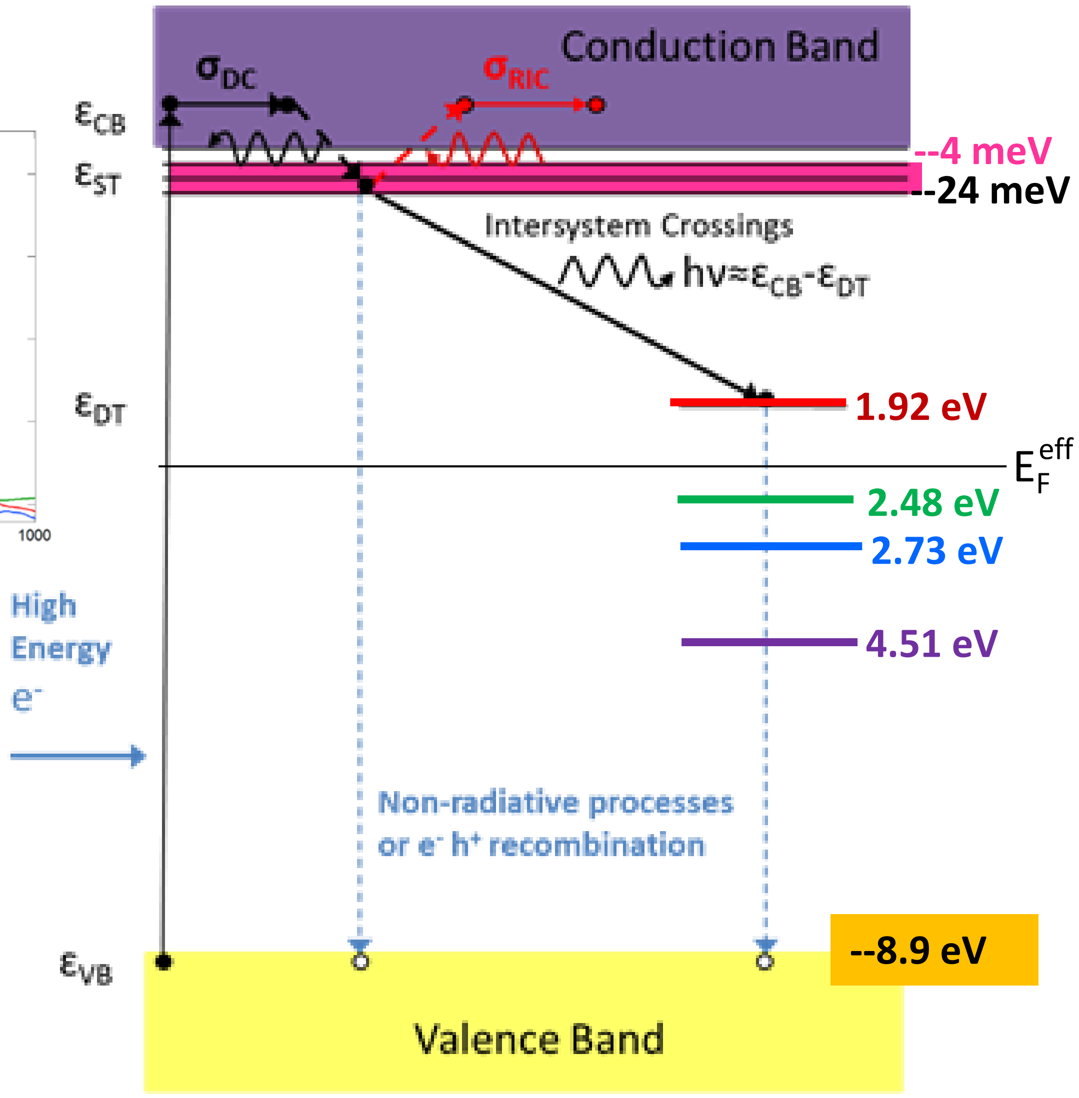

Multiple peaks in spectra correspond to multiple DOS distributions

Peak positions ⇔ Center of DOS
Peak amplitude ⇔ N_T
Peak width ⇔ DOS width

Cathodoluminescence—Defect Origins for DOS's

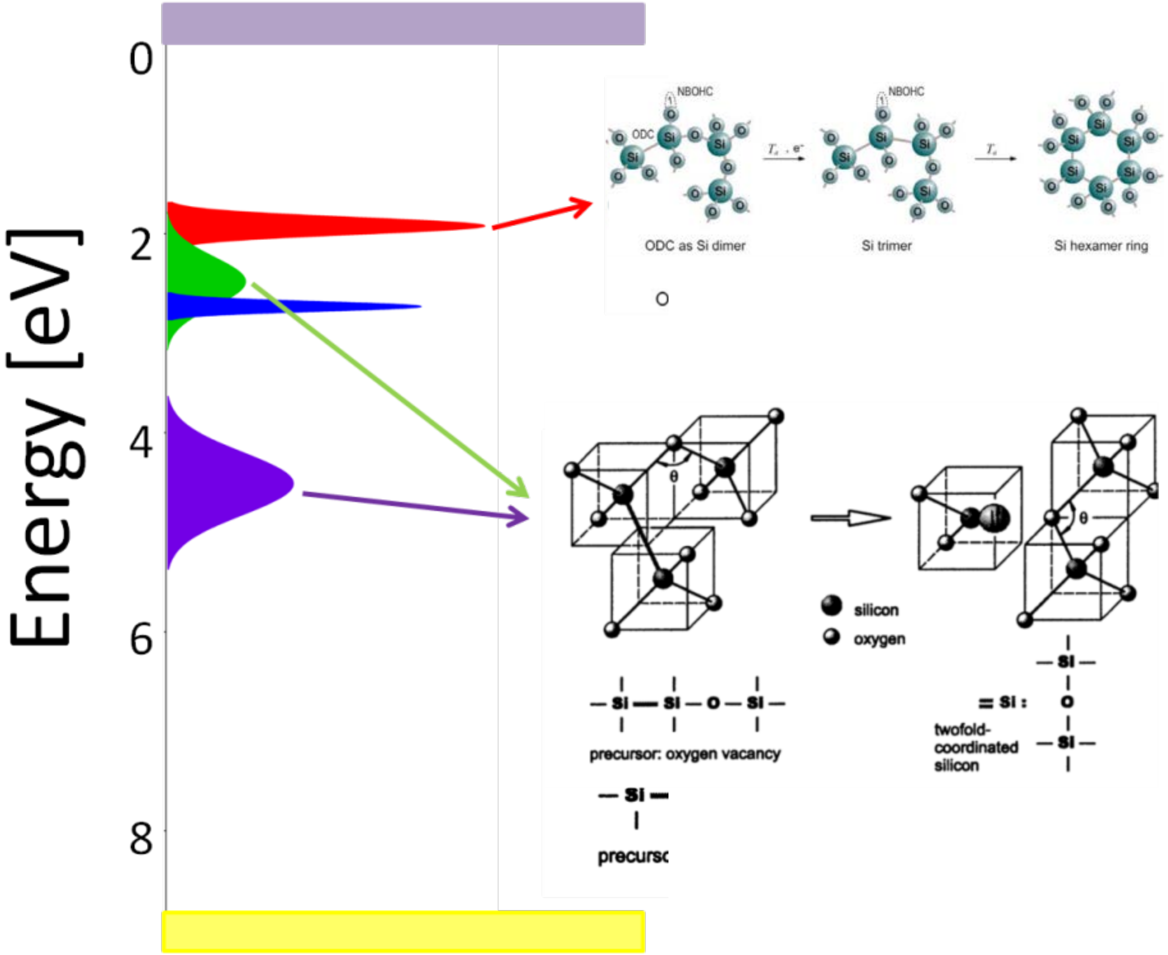

Based on peak positions for similar disordered SiO_2 samples at room temperature.

Sahl identified 1.98 eV peak as from nonbridging oxygen hole center.

Trukhin identified 2.48 eV and 4.51 eV peaks as from an oxygen deficient center.

Electron Emission Studies and DOS

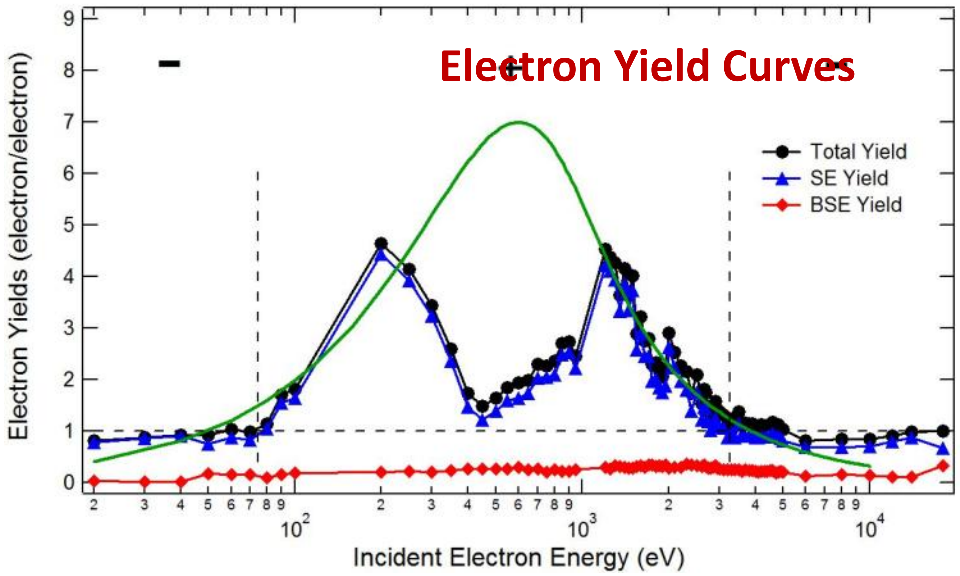

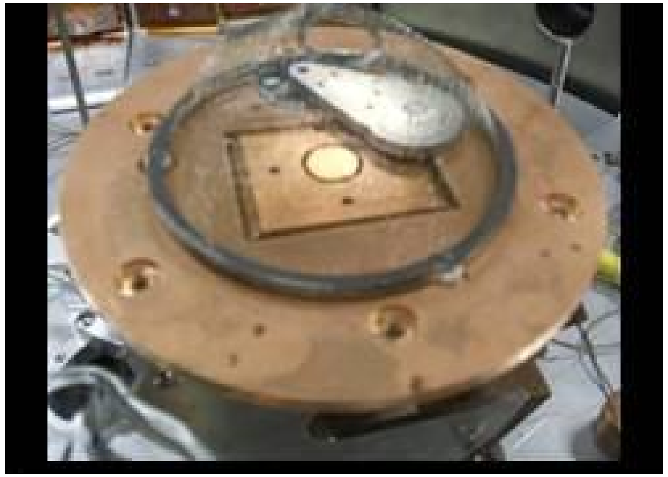

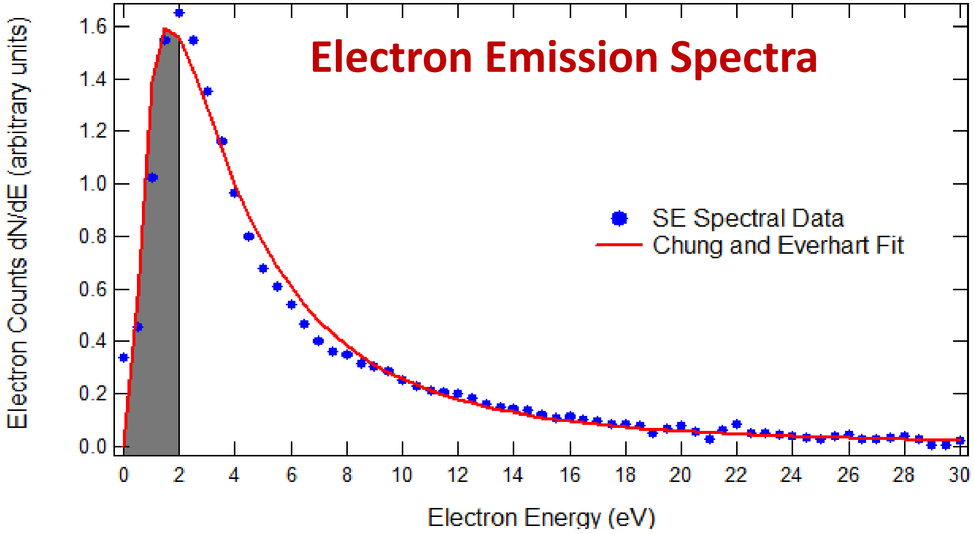

Surface Voltage Decay Curves

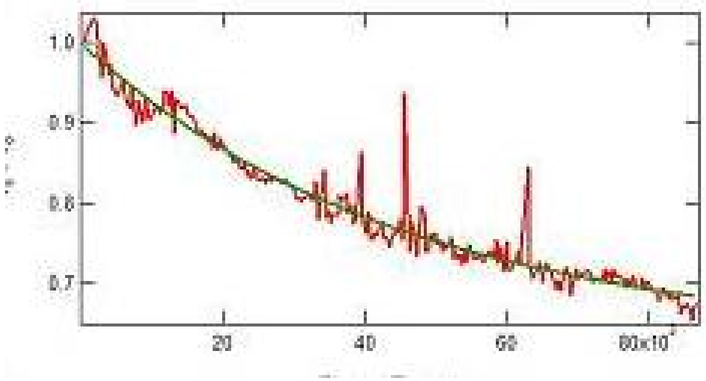

Putting the Pieces Together

Focus on DOS:

- **Synthesis of results** from different studies and techniques

- Development of **overarching theoretical models** allow extension of measurements made over limited ranges of environmental parameters to make predictions for broader ranges encountered in space.

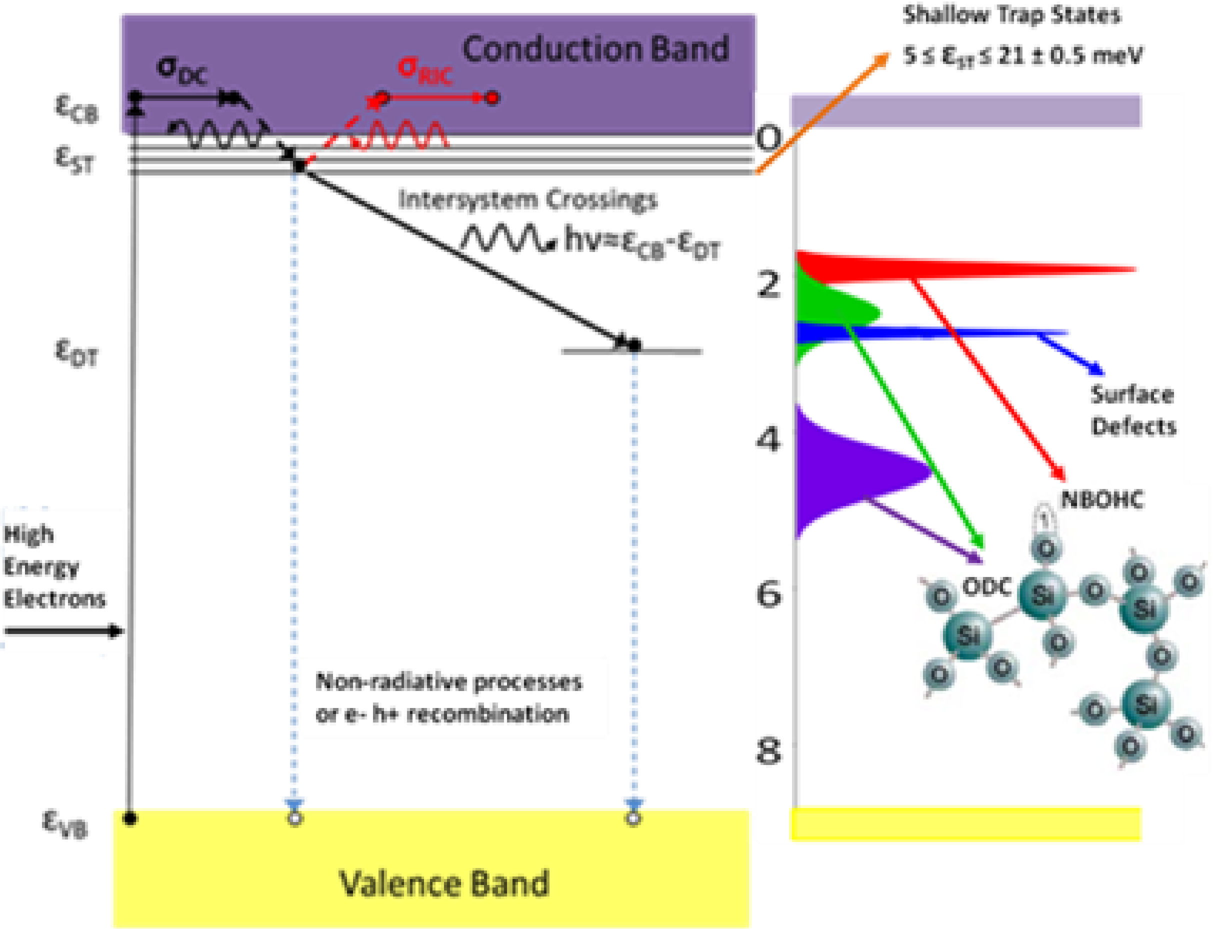

Band	Peak	Peak	FWHM	Defect	Ref.
Red	1.93±0.01 eV	663±3 nm	42 nm	NBOHC	[16,20,23]
Green	2.48±0.03	506±7	68	ODC	[17,23]
Blue	2.76±0.03	450±5	11	Surface	[18-20,23]
UV	4.97	275	50	ODC	[17-20,23]

USU Materials Physics Group

(Back row Left to Right) Ben Russon, Heather Zollinger, Zack Gibson, Matthew Robertson, Jordan Lee, David King

(Front row Left to Right) Justin Christensen, Alexandra Hughlett, Alex Souvall, Greg Wilson, Allen Andersen, JR Dennison, Windy Olsen

(Not pictured) Brian Wood, Vladimir Zavyalov, Jodie Gillespie, Jonh Mojica Decena, Katie Gamaunt, Davis Muhwezi, Tyler Kippen

USU MPG Webpage

http://digitalcommons.usu.edu/mp/

J. R. Dennison received the B.S. degree in physics from Appalachian State University, Boone, NC, in 1980, and the M.S. and Ph.D. degrees in physics from Virginia Tech, Blacksburg, in 1983 and 1985, respectively. He was a Research Associate with the University of Missouri—Columbia before moving to Utah State University (USU), Logan, in 1988. He is currently a Professor of physics at USU, where he leads the Materials Physics Group. He has worked in the area of electron scattering for his entire career and has focused on the electron emission and conductivity of materials related to spacecraft charging for the last two decades.

USU Space Survivability Test Chamber

Utah NASA Space Grant Consortium Faculty Research Infrastructure Award Program, “Space Survivability Test Facility for CubeSats, Components and Spacecraft Materials,” JR Dennison, (April 2016 to April 2017.

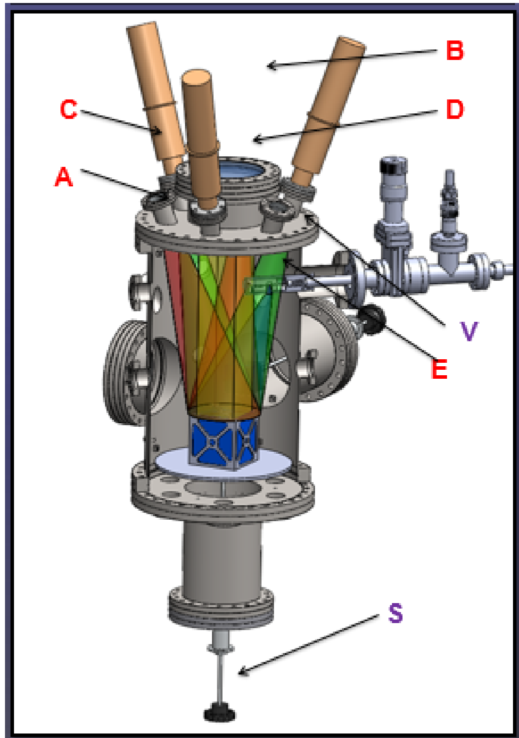

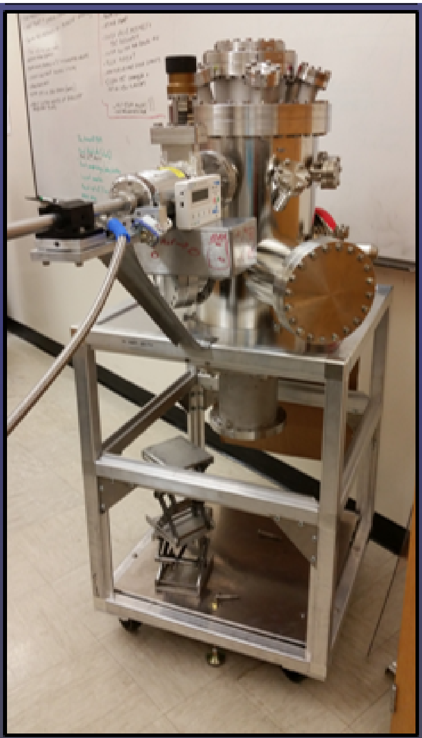

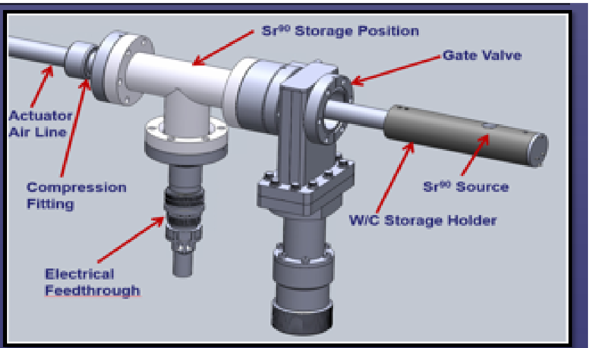

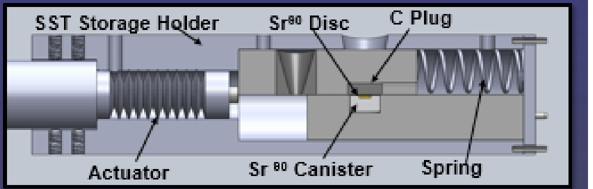

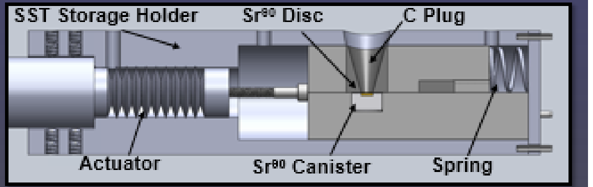

Radiation Sources
- A High Energy Electron Gun
- A' Low Energy Electron Gun
- B UV/NIS/NIR Solar Simulator
- C FUV Kapton Discharge Lamps
- D Air Mass Zero Filter Set
- E Flux Mask
- E' Sr^{90} Radiation Source

Analysis Components
- F UV/VIS/NIR Reflectivity Spectrometers
- G IR Emissivity Probe
- H Integrating Sphere
- I Photodiode UV/VIS/NIR Flux Monitor
- J Faraday Cup Electron Flux Monitor
- K Platinum Resistance Temperature Probe

Sample Carousel
- L Samples
- M Rotating Sample Carousel
- N Reflectivity/Emissivity Calib. Standards
- O Resistance Heaters
- P Cryogen Reservoir

Chamber Components
- Q Cryogen Vacuum Feedthrough
- R Electrical Vacuum Feedthrough
- S Sample Rotational Vacuum Feedthrough
- T Probe Translational Vacuum Feedthrough
- U Sapphire UV/VIS Viewport
- V MgF UV Viewport
- W Turbomolecular/Mech. Vacuum Pump
- X Ion Vacuum Pump
- Y Ion/Convectron Pressure Gauges
- Z Residual Gas Analyzer

Chamber Components
- α CubeSat
- β CubeSat Test Fixture
- Γ Radiation Shielding
- Δ COTS Electronics
- ε Rad Hard Breadboard
- η COTS Text Fixture
- Θ Electron Gun

Instrumentation (Not Shown)
- Data Acquisition System
- Temperature Controller
- Electron Gun Controller
- UV/VIS/NIR Solar Simulator Controller
- FUV Kr Resonance Lamp Controller
- Spectrometers and Reflectivity Source

UNSGC 2016 Infrastructure Grant

Simulated Space Environment Fluxes

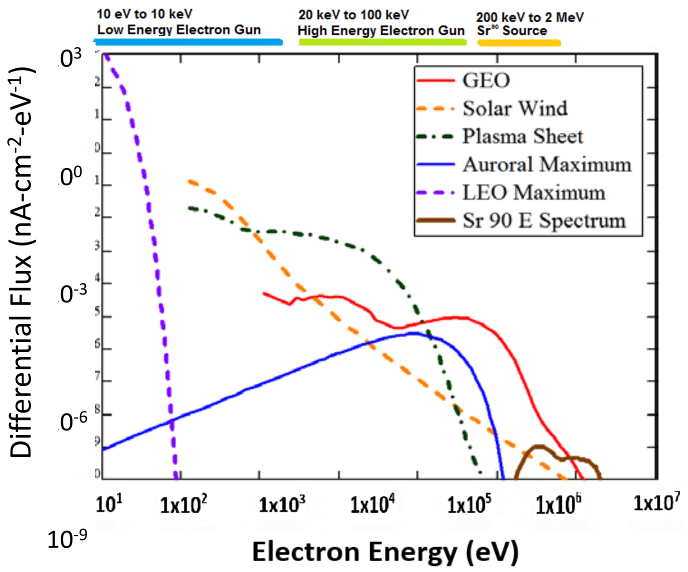

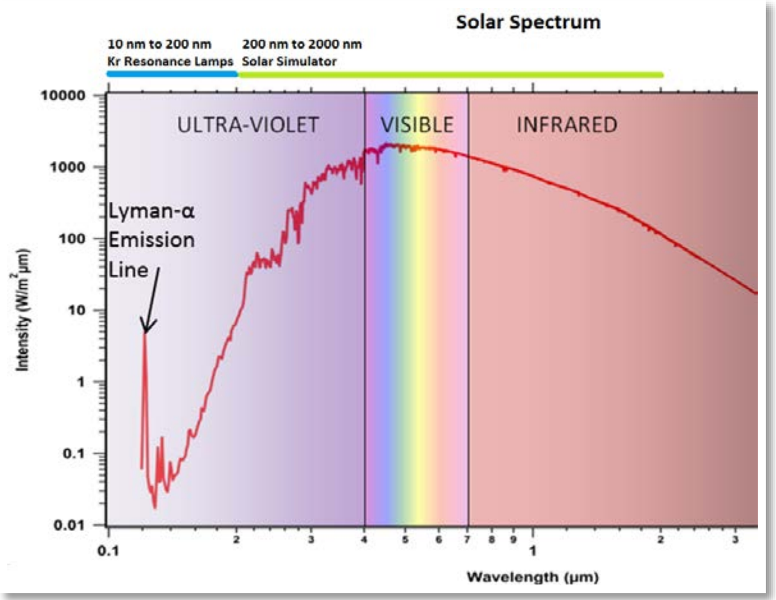

Electron Radiation

A high energy (~10-80 keV) and three lower energy (~10 eV to 5 keV) electron guns provide high electron fluxes.

Ionizing Radiation

A 100 mCi encapsulated Sr^{90} β-radiation source (~200 keV to >2.5 MeV) mimics high energy (~500 keV to 2.5 MeV) geostationary electron flux [2].

Infrared/Visible/Ultraviolet Flux

A commercial Class AAA solar simulator provides NIR/Vis/UVA/UVB electromagnetic radiation (from 200 nm to 1700 nm) at up to 4 times sun equivalent intensity.

Far Ultraviolet Flux

Kr resonance lamps provide FUV radiation flux (ranging from 10 to 200 nm) at 4X sun equivalent intensity. Kr bulbs have ~3 month lifetimes for long duration studies.

Temperature Control

Temperature range from 60 K [4] to 450 K is maintained to ±2 K [3]. This is achieved through cartridge heaters, and chilled fluid pumped through a cold plate.

Controlled Atmosphere and Vacuum

Ultrahigh vacuum chamber allows for pressures $<10^{-7}$ Pa to simulate LEO.

Video Discharge Monitoring

Using custom developed software, live video capture and processing of electrostatic discharge events allows for visual identification of discharge location and frequency.

Flexible Sample Mounting

A rotating graphite carousel, ensures uniform irradiation and allows for custom mounting of samples. Or a flange mounted fixture allows for electrostatic discharge testing. Radiation source to sample distance is adjustable.

Biological Testing

Biological samples, which are vacuum incompatible, can use a custom designed chamber with controlled atmosphere and temperature.